Quaternary International 482 (2018) 27–45

Contents lists available at ScienceDirect

Quaternary International

journal homepage: www.elsevier.com/locate/quaint

# Tectonic controls on the stratigraphic development of the rifted Taipei Basin: A late quaternary marine-influenced inland half graben

Pin-Ju Su[a,b], Andrew Tien-Shun Lin[c,*], Jyr-Ching Hu[a], Louis Shu-Yu Teng[a]

[a] Institute of Geosciences, National Taiwan University, No. 1, Sec. 4, Roosevelt Rd., Taipei, 10617, Taiwan, Republic of China
[b] Central Geological Survey, No. 2, Ln. 109, Huaxin St., Zhonghe Dist., New Taipei, 235, Taiwan, Republic of China
[c] Department of Earth Sciences, National Central University, No. 300, Zhongda Rd., Zhongli Dist., Taoyuan, 32001, Taiwan, Republic of China

ARTICLE INFO

*Keywords:*
Basin subsidence
Rift basin
Stratigraphic development
Eustatic fluctuation
Sediment supply
Taipei Basin

ABSTRACT

We establish the three-dimensional stratigraphic architecture of the Taipei Basin and its spatiotemporal palaeoenvironmental development during the past 50 kyr by analysing 36 borehole cores and 177 age dates. We calculate the rates of basin subsidence from the borehole data at depths where radiocarbon age dates are available. Our results indicate that, during the eustatic sea level falling period (35–20 ka), low rates of sediment supply and/or rapid basin subsidence controlled sedimentation, leading to a change in the depositional environment from gravelly braided rivers, through sandy braided rivers, to meandering rivers with falling eustatic sea level. During the early stage of eustatic sea level rise (~20–10.2 ka), balanced rates of sediment supply, eustasy and basin subsidence maintained the meandering river environment. Rapid sea level rise led to the initial appearance of estuarine facies at ~10.2 ka and widened the distribution of the estuarine environment after 8.5 ka; however, the coeval phases of rapid basin subsidence ~10.6–10.2 ka and 9–8.5 ka promoted the first appearance and widening of the estuary, respectively. After 7 ka, when the eustatic sea level and rate of basin subsidence remained relatively stable, sufficient sediment supply gradually infilled the estuary. The established stratigraphy improves our understanding of the factors controlling stratigraphic development in marine-influenced inland half grabens, specifically in the Taipei Basin with high rates of sediment supply. Accommodation space in the Taipei Basin was governed by eustatic fluctuations with modulations by basin subsidence and sediment supply since the last glacial period.

## 1. Introduction

Rising eustatic sea level since the last glacial period has promoted the appearance of estuaries along coastlines worldwide, thus emphasising the importance of studying estuarine environments. The vertical variation in the fluvial–estuarine–fluvial tripartite model proposed by Roy et al. (1980) is widely accepted. Furthermore, conceptual models of stratigraphic stacking patterns for both wave-dominated (Roy, 1984; Dalrymple et al., 1992) and tide-dominated (Dalrymple et al., 1992) estuaries have been established. Recent studies have focused on the factors controlling palaeoenvironmental changes (e.g. Ricci Lucchi et al., 2006; Granja et al., 2010; Tesson et al., 2011; Amato et al., 2013; Milli et al., 2013; Traini et al., 2013) and stratigraphic architectures (e.g. Hori et al., 2001; Anthony et al., 2002; Holz, 2003) on tectonically stable coasts, as well as in tectonically active areas (e.g. Willis, 2000; Wilson et al., 2007; Gobo et al., 2014). Although previous works have studied the tectonic controls on estuarine stratigraphy (e.g. Ricci Lucchi et al., 2006; Granja et al., 2010; Tesson et al., 2011), little attention has been paid to the interplay between tectonic subsidence/uplift and eustatic fluctuations (Tanabe et al., 2013).

The Taipei Basin is an active rift basin located 10 km inland from the coast of northern Taiwan (Fig. 1). The basin is connected to the sea through a river channel, which resulted in the development of a brackish environment during the Holocene transgression (Wang-Lee et al., 1987; Peng et al., 1999; Teng et al., 2000). The post-50-kyr basin fill records a complete sedimentary cycle with a vertical stacking pattern characterised by a fluvial–estuarine–fluvial tripartite facies distribution. Comprising well-preserved sediments, with an excellent age constraint, as well as well-established eustatic sea level curves for the past 50 kyr, the Taipei Basin is an ideal natural laboratory for studying the interplay between tectonics, eustatic changes and sediment supply.

We first establish the spatiotemporal palaeoenvironmental framework for the Taipei Basin based on sedimentary facies analysis of 36 evenly distributed borehole cores and 173 radiocarbon age dates and 4 thermoluminescence age dates. Basin subsidence is then calculated for each dated horizon in the studied boreholes, using input parameters of

* Corresponding author.
*E-mail address:* andrewl@ncu.edu.tw (A.T.-S. Lin).

https://doi.org/10.1016/j.quaint.2018.04.028
Received 30 October 2017; Received in revised form 28 March 2018; Accepted 14 April 2018
Available online 17 April 2018
1040-6182/ 

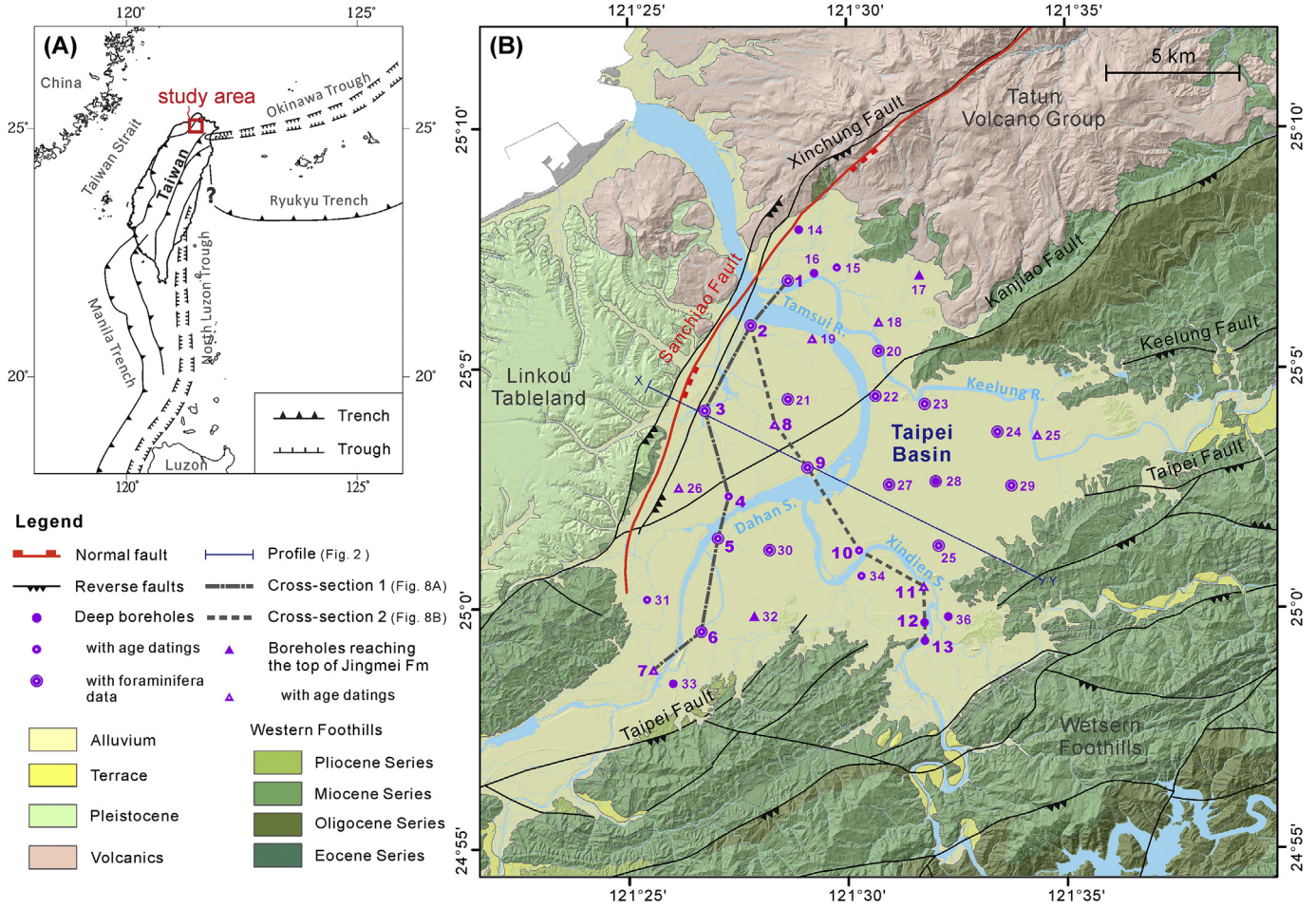


**Fig. 1.** Tectonic framework of Taiwan and geological provinces in the Taipei Basin study area. (A) Regional tectonic setting of Taiwan; the study area is marked by a red rectangle. (B) Geological map of the study area in the Taipei Basin. The locations of boreholes, one stratigraphic profile (X–Y profile shown in Fig. 2) and two well-correlation cross sections (N–S-oriented boreholes 1–7 and NW–SE-oriented boreholes 2–13) are also shown. Circles represent boreholes penetrating through the Jingmei Fm; triangle symbols indicate boreholes reaching the top of the Jingmei Fm. R: river, S: stream. (For interpretation of the references to colour in this figure legend, the reader is referred to the Web version of this article.)

sampled depth, eustatic sea level and palaeowater depth, to determine the spatiotemporal variations in basin subsidence during the past 50 kyr. We finally discuss the effects of interplay between tectonic subsidence, eustasy and sediment supply on sedimentation in the Taipei Basin. Our study yields insights into sedimentation in an active marine-influenced inland half graben.

## 2. Geological background

The Taipei Basin covers an area of 243 km$^2$ and is located within the northern Taiwan orogenic belt, resulting from the convergence between the Eurasian Plate and the Philippine Sea Plate. Several NE–SW-striking and inactive reverse faults are distributed in the mountains surrounding the basin (Fig. 1). The steep southeast-dipping Sanchiao Fault (Chen et al., 2014) is the major basin-bounding normal fault along the western margin of the Taipei Basin (Shih et al., 2006) and is considered to be an active fault (Lin et al., 2007) with a probable listric fault geometry at depth (Chen et al., 2010a). It separates the basin from the Pleistocene Linkou Tableland to the west. Several volcanic complexes occur in the fold-and-thrust belt to the north of the basin. To the east and south of the basin lie the Western Foothills, consisting of Paleogene to Neogene sedimentary rocks, which constitute the basin substrate. The basement surface of the Taipei Basin dips to the northwest towards the Sanchiao Fault, displaying a half-graben basin geometry (Teng et al., 2001).

The Taipei Basin connects to the Taiwan Strait in the west through a 10-km-long stretch of the Tamsui River. The tidal range at the river mouth is approximately 2 m, and tidal currents intrude into the basin up to 20 km inland along the tributaries (Chang et al., 1989; Hsu et al., 2006). Three tributary systems, i.e. the Dahan Stream, Keelung River and Xindien Stream, transport sediments into the basin from the surrounding mountains (Fig. 1).

The Late Pleistocene to Holocene basin fill is up to ~680 m thick and comprises three sedimentary cycles (Teng et al., 2000) covering the past 0.4 Myr (Tsao et al., 1999; Teng et al., 2008). Teng et al. (1994) identified four lithostratigraphic units, namely the Banchiao Fm, Wuku Fm, Jingmei Fm and Sungshan Fm (in ascending order; Fig. 2). These four formations all dip and thicken to the northwest towards the Sanchiao Fault.

The final sedimentary cycle, comprising the Jingmei Fm and the Sungshan Fm, was deposited during the past 50 kyr. The Jingmei Fm represents sedimentation after the Dahan Stream was captured approximately 50 ka, and the Tamsui river system has experienced negligible changes since then (Teng et al., 2004). The total stratal thickness of these two formations is up to ~140 m, comprising the ~30-m-thick Jingmei Fm and the ~110-m-thick Sungshan Fm, in the northwest corner of the basin. The Jingmei Fm consists of alluvial-fan gravels (Peng et al., 1999; Hong et al., 2006) erosively overlying the sand-prone Wuku Fm. In the southern and southeastern parts of the basin, the composition of the Wuku Fm becomes gravel-rich, such that the contact between the Jingmei Fm and the Wuku Fm is difficult to identify. The

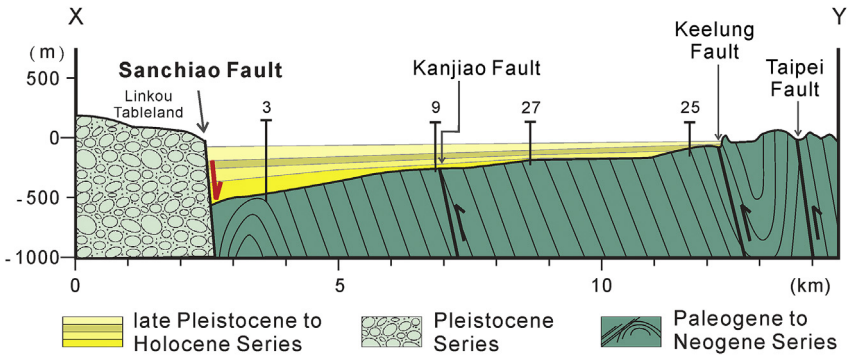


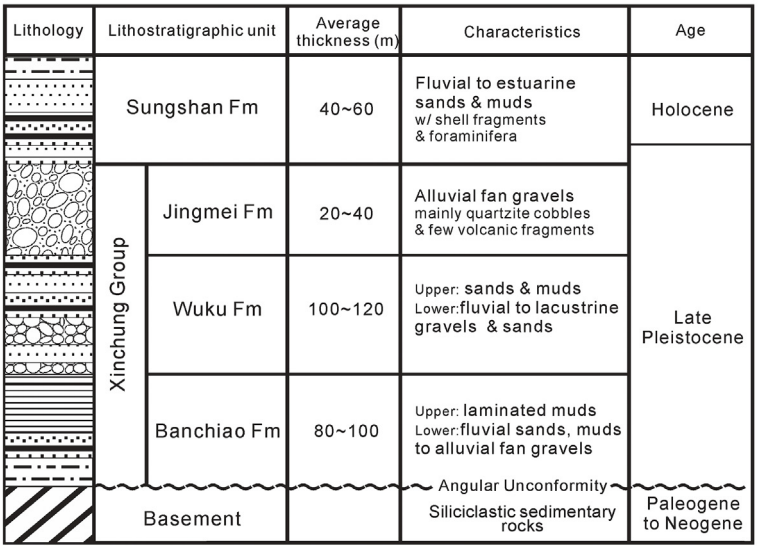


**Fig. 2.** Schematic cross section across the Taipei Basin and basin stratigraphy. (A) WNW–ESE-oriented structural and stratigraphic profile across the Taipei Basin showing the basin geometry and major stratigraphic units, the Linkou Tableland and the underlying basement (see Fig. 1B for profile location). The Sanchiao Fault is an active basin-bounding fault, with slip sense indicated by a red arrow. (B) Stratigraphy and characteristics of the late Quaternary basin-fill sediments in the Taipei Basin (modified after Teng et al., 2000). (For interpretation of the references to colour in this figure legend, the reader is referred to the Web version of this article.)

Sungshan Fm, consisting of fluvial to estuarine sands and muds (Huang, 1962; Peng et al., 1999; Hong et al., 2006), can be easily distinguished from the underlying, gravel-rich Jingmei Fm.

Volcaniclastics, derived from the Tatun Volcano Group to the north of the basin, are preserved mostly in the Banchiao Fm and the Wuku Fm (Chen and Lin, 2000). Several volcaniclastic layers observed in the lower part of the Sungshan Fm are interpreted as either reworked sediments (Chen and Lin, 2000) or lahars (Tsao et al., 2001; Song et al., 2007). Since these layers are neither related to volcanic activity nor affected the sedimentation in the basin, they are not discussed in this study.

## 3. Materials and methods

Thirty-six continuously cored boreholes, which are distributed evenly throughout the Taipei Basin and were drilled by the Central Geological Survey (CGS) during 1992–2014, are described sedimentologically in this study (Fig. 1). The borehole lengths are between 35 m and 760 m, and the core-recovery rates are all greater than 95%. All the cores were sectioned into halves and have been preserved in the CGS storehouses. The archived halves are for continuous visual sedimentological descriptions and the working halves are for sampling.

The sedimentological descriptors for each core include grain size, sedimentary structures, fossils, accessory materials (e.g. vivianites, wood fragments, plant remains and carbonaceous materials) and color. Grain size description follows the classification of Wentworth (1922). Published foraminiferal studies are reported for 16 boreholes (Shieh, 2001, 2006; Huang, 2006) and are also integrated with lithofacies for palaeoenvironmental interpretation. An example lithological column is displayed in Fig. 3. Of the 36 analysed boreholes, 13 have been selected to illustrate the spatiotemporal lithofacies variations across the basin. Eleven of these selected boreholes penetrate through the base of the Jingmei Fm and the other two boreholes (nos. 8 and 10) reach the top several metres of the Jingmei Fm. The studied depth is to the base of the Jingmei Fm, ranging from 32 m to 143 m below the ground surface.

From 27 of the boreholes, 177 samples of wood fragments, plant remains and shells were collected for accelerator mass spectrometry (AMS) radiocarbon dating to establish the age–depth models for these cores (e.g. Fig. 3, right-hand panel). Of the 177 dating results, 7 are reported for the first time in this study and were dated by Beta Analytic Inc. (Table 1). The rest of the ages are collated from previous studies (Liu et al., 1994; Liu, 1995; Tseng and Liew, 1999; Hong et al., 2006; Su et al., 2018). In addition to reworked samples, shell samples are preferentially excluded as opposed to terrestrial samples (i.e. plant remains and carbonaceous muds) because of their uncertain local marine reservoir correction (ΔR) value (Stuiver and Braziunas, 1993). Sixty-two AMS radiocarbon dates and an additional four thermoluminescence dates (Wei et al., 1998) from eleven boreholes in the cross sections are listed in Table 1. All available radiocarbon ages are re-calculated and correlated using the CALIB 7.0.4 program (Stuiver et al., 2016), referring to the IntCal13 or Marine13 calibration curves (Reimer et al., 2013).

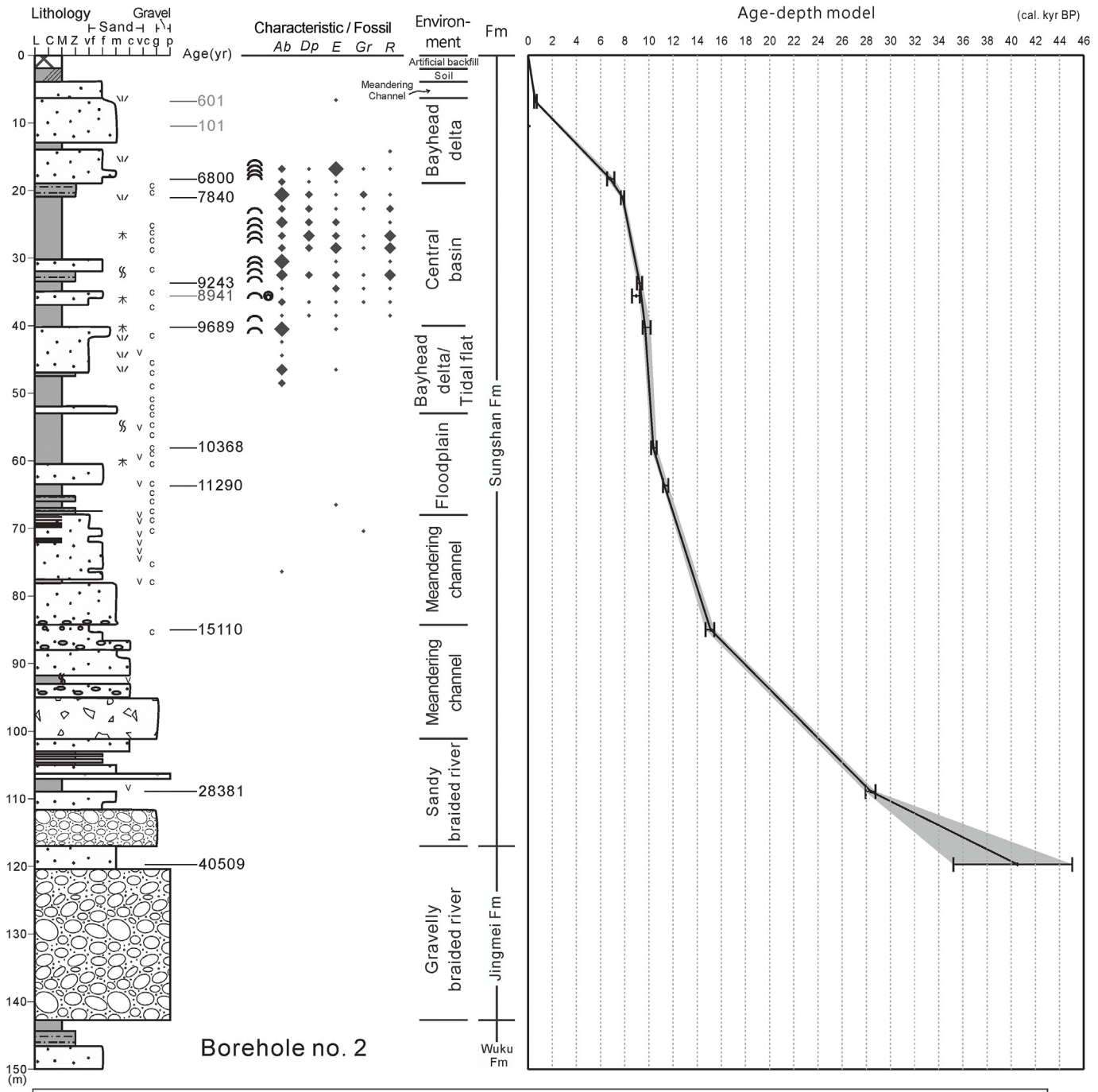


**Foraminifera abundance**

- amount 1~9 individuals
- amount 10~19 individuals
- amount 20~39 individuals
- amount >40 individuals

*Ab: Ammonia beccarii* vars.
*Dp: Discorbis praegeri*
*E: Elphidium* spp.
*Gr: Globigerinoides ruber*
*R: Rosalina* spp.

**Lithology**

- gravel
- sand
- silt
- mud
- volcaniclastics
- soil
- artificial backfills
- mud clast
- granule or pebble

**Other characteristics**

- shells (and fragments)
- oysters (and fragments)
- plant remains
- vivianites
- bioturbation
- wood fragments
- c carbonaceous materials
- 6800 radiocarbon age (years B.P.)

*(caption on next page)*

**Fig. 3.** Representative stratigraphic and sedimentological column with palaeoenvironmental interpretations, using borehole no. 2 as an example (see Fig. 1B for borehole location). Selected representative species of foraminifera (*Ab, Dp, E, Gr* and *R*) identified by Huang (2006) are noted. Radiocarbon ages are expressed as median values alongside the stratigraphic column. The detailed radiocarbon age dates for this borehole can be found in Table 1. Ages shown in light grey are considered to be unreliable as they are obtained from reworked material or shell fragments. The age–depth model is shown in the right-hand column. The solid black curve connects the mean age for each data point and the grey area is the 95% confidence interval.

## 4. Facies analyses and facies associations

Seven facies associations of fluvial and estuarine depositional systems are identified from the sediments of the Jingmei Fm and the Sungshan Fm (Fig. 4). Detailed facies descriptions and interpretations for these two formations have been documented by Su et al. (2016) and Su et al. (2018), respectively. Here, we outline the palaeoenvironmental interpretations and overall stratigraphic architectures (Tables 2 and 3).

### 4.1. Gravelly braided river (GB) facies association

The GB facies association comprises the Jingmei Fm and is widely distributed throughout the basin, except to the north of the Keelung River (Fig. 5). It is approximately 20–30 m thick and thins northward. The maximum thickness is 60 m, which occurs in the western part of the basin near borehole no. 4. This facies association consists of clast-supported and sub-rounded gravels pertaining to the Gc lithofacies (Tables 2 and 3, Fig. 6A). The grain diameter of the gravels is 3–6 cm, although some are larger than 10 cm, and the grain size decreases towards the north. The matrix is yellowish-brown and comprises mainly medium-to coarse-grained sands, but these are seldom preserved in the cores due to washing out during drilling.

We interpret that the GB facies association is of fluvial origin since it contains no marine fossils or foraminifera. The gravel sizes indicate strong and competent tractional flows. A lack of interbedded fine-grained sediments (i.e. mud) indicates a high-energy environment or that fine material may have been removed by the competent flows. The gravels were deposited in braided rivers with limited overbank deposits, as shown by Miall and Arush (2001). The yellowish-brown color of the gravels and matrix sands indicates weathering due to subaerial exposure. Therefore, the GB facies association was most likely deposited in gravelly braided rivers on alluvial fans.

### 4.2. Sandy braided river (SB) facies association

The 6–10-m-thick SB facies association occurs in the lower Sungshan Fm, above the GB facies association, in the western part of the basin (Fig. 5). It also occurs in the upper Sungshan Fm, sharply overlying the floodplain (FL) facies association (see Section 4.4) or tidal flat (TF) facies association (see Section 4.7) in the southern and southeastern parts of the basin, respectively. It comprises grey to yellowish-grey, medium-to very coarse-grained sands (Sm) and small sub-rounded pebbles (Smg) with diameters ranging from 1 cm to 3 cm (Fig. 6B).

The lack of interlayered mud or smaller grain-size sediments than the gravels of the Gc lithofacies suggests that these lithofacies were deposited downstream of the gravelly braided river environment. The SB facies association is characteristic of sandy braided channels, where the massive sands may represent sandbars.

### 4.3. Meandering channel (CH) facies association

The CH facies association is laterally discontinuous, with an average thickness of 5–25 m, and occurs in the lower and top parts of the Sungshan Fm (Fig. 5). It comprises massive sands (Sm), horizontal-laminated sands (Sh), cross-laminated sands (Sx) and matrix-supported granules and mud clasts (Smg). The dominant lithofacies is Sm, which consists of grey to yellowish-grey, fine-to medium- or coarse-grained and structureless sands, whereas lithofacies Sh and Sx occur occasionally (Fig. 6C). This facies association is floored by an erosional surface, overlain by lag deposits consisting of granules to small pebbles and mud clasts (Smg). It shows a fining-upward trend from coarse-to medium-grained sands at the bottom to very fine sands or muds at the top. Plant remains, few wood fragments and bioturbation are observed in the fine-grained sediments.

The physical characteristics and vertical stacking of lithofacies are typical of channel deposits (e.g. Anthony et al., 2002; Rossetti and Santos Júnior, 2004; Ricci Lucchi et al., 2006; Hijma et al., 2009), and a lack of shell fragments, foraminifera and indicative tidal structures further indicates deposition in a fluvial channel. Since the CH facies association is commonly encased in thick muds of the FL facies association (see below), we interpret a meandering channel environment.

### 4.4. Floodplain (FL) facies association

The FL facies association occurs mostly in the bottom and top parts of the Sungshan Fm, similar to the CH facies association distribution (Fig. 5). Its total thickness range is 5–40 m in the lower Sungshan Fm and 5–10 m in the upper Sungshan Fm. It comprises massive muds and finely laminated muds and silts (Mm), occasionally with beds of horizontally laminated silts to fine sands (Sh) (Fig. 6D). The muds are usually grey in color but sometimes exhibit yellowish-brown to reddish-brown bands. Plant remains, wood fragments, carbonaceous materials and vivianites occur frequently.

The FL facies association appears to be associated with the CH facies association. The fine-grained sediments indicate a low-energy environment, most likely a floodplain or swamp. Abundant wood fragments, plant remains and carbonaceous materials are derived from floodplain or river catchment vegetation. Furthermore, the presence of carbonaceous materials can be considered to have promoted the formation of authigenic vivianite, as this mineral is known to favour lower-energy environments with reducing redox (Rosenquist, 1970) and alkaline (Rosenquist, 1970; Nriagu, 1972) conditions and low sediment accumulation rates (Rosenquist, 1970; Nriagu, 1972; Fagel et al., 2005). The yellowish-brown to reddish-brown bands are likely the result of subaerial weathering since floodplain and swamp sediments are sporadically exposed (Anthony et al., 2002; Kitazawa, 2007). The presence of the Sh lithofacies within the thick muds indicates occasional flooding events in this depositional system (Nichols and Fisher, 2007).

### 4.5. Bayhead delta (BD) facies association

The BD facies association has a thickness of 5–15 m and occurs in the upper and middle parts of the Sungshan Fm (Fig. 5). It is associated vertically and laterally with the CB facies association, indicating that these two facies associations were deposited in adjacent environments. It comprises grey, fine- to coarse-grained and massive sands (Sm); horizontally laminated sands (Sh); cross-laminated sands (Sx) and heterolithic beds with flaser to wavy bedding (SMh) (Fig. 7B). In some cores, the uppermost part of this facies association may become yellowish-brown in color. The constituent lithofacies also contain plant remains, wood fragments, shell fragments and few foraminifera. Some large, intact shell fragments, such as *Placuna placenta*, can be recognised in the Sm lithofacies, and the foraminiferal species are mostly *Ammonia beccarii* and *Elphidium* spp. Biogenic structures are occasionally present in the SMh and Sm lithofacies. Furthermore, the BD facies association shows coarsening-upward successions overlying the central basin (CB) facies association, whereas fining-upward successions are observed

**Table 1**
List of radiocarbon ages for boreholes displayed in the two cross sections, as shown in Fig. 8. Age data from the Wuku Fm is also listed for reference.

| Core No. | Sampled depth (m) | Fm[#] | Lab number | Material dated | Conventional age (yr BP) | | Calibrated age 2σ (cal yr BP) | | | Data Source[*] |
|---|---|---|---|---|---|---|---|---|---|---|
| 1 | 38.7 | Ss | Beta-355402 | shell | 7850 | ± 40 | 8845 | – | 8543 | a |
| | 94.0 | Ss | | | 21390 | ± 150 | 25981 | – | 25385 | f |
| | 101.8 | Ss | | | 26140 | ± 160 | 30836 | – | 29895 | f |
| | 114.5 | Ss | | | 33410 | ± 290 | 38493 | – | 36748 | f |
| | 156.4 | Jm-Wk | | | 37420 | ± 1520 | 44181 | – | 38712 | f |
| 2 | 6.8 | Ss | | | 610 | ± 95 | 729 | – | 496 | f |
| | 10.3 | Ss | NTU-3184 | plant fr. | 101.7 | ± 0.6 pMC | 253 | – | 33 | c |
| | 18.3 | Ss | NTU-3176 | plant fr. | 5960 | ± 90 | 7148 | – | 6555 | c |
| | 21.2 | Ss | NZA-5750 | plant fr. | 7010 | ± 80 | 7968 | – | 7682 | c |
| | 33.8 | Ss | NZA-5751 | plant fr. | 8260 | ± 90 | 9449 | – | 9023 | c |
| | 35.7 | Ss | NTU-3169 | shell fr. | 8060 | ± 100 | 9259 | – | 8636 | c |
| | 40.4 | Ss | NTU-3173 | shell fr. | 8680 | ± 100 | 10132 | – | 9489 | c |
| | 58.1 | Ss | NZA-5752 | plant fr. | 9180 | ± 100 | 10644 | – | 10183 | c |
| | 63.8 | Ss | NZA-5753 | plant fr. | 9860 | ± 80 | 11612 | – | 11144 | c |
| | 85.1 | Ss | NZA-5754 | plant fr. | 12700 | ± 90 | 15418 | – | 14699 | c |
| | 109.1 | Ss | NZA-5755 | plant fr. | 24350 | ± 180 | 28755 | – | 27952 | c |
| | 119.6 | Jm | NTU-3187 | plant fr. | 36500 | ± 2600 | 45051 | – | 35222 | c |
| | 120.8 | Jm | NZA-5756 | plant fr. | > 49500 | | | | | c |
| | 163.7 | Wk | NTU-3182 | plant fr. | > 50000 | | | | | c |
| 3 | 10.2 | Ss | Beta-92240 | – | 3610 | ± 50 | 4084 | – | 3731 | e |
| | 24.8 | Ss | NZA-3991 | plant fr. | 7160 | ± 70 | 8160 | – | 7851 | b |
| | 36.6 | Ss | NZA-3992 | plant fr. | 7560 | ± 70 | 8514 | – | 8196 | b |
| | 42.2 | Ss | NTU-1954 | plant fr. | 7930 | ± 60 | 8985 | – | 8608 | b |
| | 49.8 | Ss | NTU-1946 | plant fr. | 9010 | ± 110 | 10478 | – | 9742 | b |
| | 50.3 | Ss | NTU-1903 | plant fr. | 8660 | ± 80 | 9903 | – | 9503 | b |
| | 54.9 | Ss | NTU-1863 | plant fr. | 9090 | ± 60 | 10476 | – | 10170 | b |
| | 63.6 | Ss | NTU-1953 | plant fr. | 10180 | ± 150 | 12394 | – | 11292 | b |
| | 67.7 | Ss | NTU-1955 | plant fr. | 9530 | ± 60 | 11106 | – | 10607 | b |
| | 68.7 | Ss | NTU-1952 | plant fr. | 10080 | ± 60 | 11967 | – | 11343 | b |
| | 74.4 | Ss | NTU-1904 | plant fr. | 9810 | ± 80 | 11600 | – | 10870 | b |
| | 80.5 | Ss | Beta-93193 | | 17380 | ± 70 | 21237 | – | 20723 | e |
| | 89.4 | Ss | NTU-1958 | plant fr. | 18950 | ± 540 | 24120 | – | 21607 | b |
| | 90.7 | Ss | Beta-93194 | | 21820 | ± 80 | 26218 | – | 25860 | e |
| | 94.1 | Ss | NTU-1905 | Plant fr. | 21300 | ± 160 | 25917 | – | 25273 | b |
| | 155.9 | Wk | | % | 100000 | ± 20000 | | | | d |
| | 177 | Wk | | % | 98000 | ± 15000 | | | | b |
| | 234.1 | Wk | | % | 86000 | ± 13000 | | | | f |
| | 251 | Wk | | % | 205000 | ± 41000 | | | | b |
| 4 | 14.15 | Ss | | wood | 5900 | ± 40 | 6841 | – | 6639 | f |
| | 26.9 | Ss | | wood | 7460 | ± 40 | 8365 | – | 8190 | f |
| | 35.6 | Ss | | wood | 8000 | ± 40 | 9009 | – | 8717 | f |
| | 47.85 | Ss | | wood | 8810 | ± 40 | 10146 | – | 9683 | f |
| | 53.88 | Ss | | wood | 9130 | ± 40 | 10405 | – | 10223 | f |
| | 60.2 | Ss | | wood | 13370 | ± 70 | 16295 | – | 15842 | f |
| | 88.9 | Jm | | wood | 20620 | ± 100 | 25195 | – | 24476 | f |
| | 117.1 | Jm | | wood | 39140 | ± 970 | 44662 | – | 41675 | f |
| 5 | 15.75 | Ss | NTU-3024 | Plant fr. | 6500 | ± 45 | 7495 | – | 7314 | b |
| | 24.25 | Ss | NZA-4680 | Plant fr. | 7860 | ± 95 | 8989 | – | 8458 | b |
| | 38.5 | Ss | NTU-3023 | Plant fr. | 8180 | ± 90 | 9434 | – | 8793 | b |
| | 45.55 | Ss | NTU-3052 | Plant fr. | 9000 | ± 40 | 10242 | – | 9940 | b |
| | 50.25 | Ss | NZA-4700 | Plant fr. | 9260 | ± 120 | 10746 | – | 10201 | b |
| | 98.85 | Jm | NZA-4651 | Plant fr. | 25300 | ± 260 | 30134 | – | 28760 | b |
| 6 | 23.05 | Ss | NZA-3111 | Plant fr. | 7950 | ± 80 | 9005 | – | 8600 | b |
| | 62.5 | Wk | NZA-3144 | charcoal | > 51400 | | | | | b |
| 7 | 17.1 | Ss | Beta-309294 | wood | 7640 | ± 40 | 8537 | – | 8381 | g |
| 8 | 25.3 | Ss | Beta-309278 | wood | 7960 | ± 40 | 8990 | – | 8649 | g |
| | 34.3 | Ss | Beta-309279 | shell fr. | 8750 | ± 40 | 9901 | – | 9564 | g |
| | 53.5 | Ss | Beta-309281 | wood | 8180 | ± 40 | 9260 | – | 9020 | g |
| 9 | 18.5 | Ss | | | 7800 | | | | | f |

(*continued on next page*)

**Table 1** (*continued*)

| Core No. | Sampled depth (m) | Fm[#] | Lab number | Material dated | Conventional age (yr BP) | | Calibrated age 2σ (cal yr BP) | | | Data Source[*] |
|---|---|---|---|---|---|---|---|---|---|---|
| 10 | 11.7 | Ss | Beta-222156 | wood | 3220 | ± 40 | 3558 | – | 3368 | a |
| | 14.8 | Ss | Beta-222157 | wood | 7290 | ± 40 | 8177 | – | 8017 | a |
| | 20.0 | Ss | Beta-222158 | Plant fr. | 7700 | ± 50 | 8581 | – | 8408 | a |
| | 24.6 | Ss | Beta-222159 | wood | 8030 | ± 50 | 9030 | – | 8659 | a |
| | 28.2 | Ss | Beta-222160 | wood | 8240 | ± 50 | 9402 | – | 9032 | a |
| | 31.7 | Ss | Beta-222161 | wood | 8600 | ± 50 | 9678 | – | 9496 | a |
| 11 | 26.4 | Ss | Beta-309295 | wood | 8200 | ± 40 | 9277 | – | 9027 | g |
| 27 | 5.8 | Ss | | | 5110 | ± 40 | 5929 | – | 5746 | f |
| | 1.15 | Ss | | | 6250 | ± 40 | 7264 | – | 7020 | f |
| | 18.5 | Ss | | | 7490 | ± 40 | 8384 | – | 8200 | f |
| | 24.15 | Ss | | | 7890 | ± 40 | 8974 | – | 8590 | f |
| | 34.6 | Ss | | | 8820 | ± 40 | 10149 | – | 9696 | f |
| | 40.3 | Ss | | | 9050 | ± 40 | 10252 | – | 10177 | f |
| | 46.5 | Ss | | | 9350 | ± 40 | 10690 | – | 10435 | f |

# abbreviations of the formations: Ss: Sungshan Fm; Jm Fm: Jingmei Fm; Wk: Wuku Fm.
*data source: a: this study; b: Liu et al. (1994); c: Liu (1995); d: Wei et al. (1998); e: Tseng and Liew (1999); f: Huang, 2006; g: Su et al. (2018). The symbol "%" means the age data are from thermoluminescence dating.

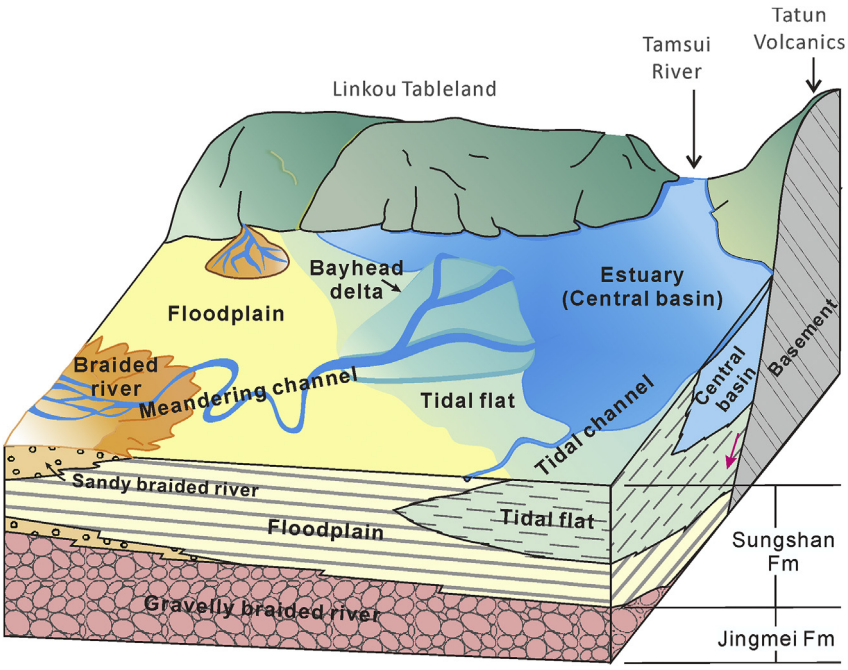


**Fig. 4.** Conceptual 3D diagram illustrating the sedimentary environments in the Taipei Basin approximately 7 ka.

beneath the CB facies association.

Since the BD facies association is confined vertically and laterally between the CB and FL facies associations, the depositional environment should lie between floodplain and estuarine central basin. We therefore interpret this facies association to represent bayhead delta deposits. The coarsening-upward successions reflect deltaic progradation (Roberts, 1998; Bos, 2010), and the occasional fining-upward successions may be due to increasing water depth during transgressions or autocyclic lateral migration of tidal channels. The yellowish-brown color of the upper successions may originate from weathering due to prolonged subaerial exposure.

### 4.6. Tidal flat (TF) facies association

The TF facies association is 5–15 m thick and occurs between the CB and FL facies associations in both the lateral and vertical directions (Fig. 5). It comprises bioturbated, grey to yellowish-grey, massive muds and silty muds with occasional occurrences of shell fragments and foraminifera (Mfm); few thin sand or silt layers with horizontal laminations (Sh); and slightly bioturbated heterolithic beds with lenticular and wavy bedding (SMh) (Fig. 7C). It also contains abundant carbonaceous materials, plant remains, wood fragments, shell fragments (*Placuna placenta*), foraminifera and some vivianites. The predominant foraminiferal species are *A. beccarii* and *Elphidium* spp.; however, the number of foraminifera is less than that in the CB facies association.

The rare and euryhaline foraminiferal species are similar to those in the BD facies association. Both associations correspond to an environment lying between estuarine central basin and floodplain. We therefore interpret that the TF facies association pertains to muddy tidal flat to salt marsh environments.

### 4.7. Central basin (CB) facies association

The CB facies association occurs only in the upper part of the middle

**Table 2**
Lithofacies descriptions and interpretations for the upper Pleistocene to Holocene sediments in the Taipei Basin.

| Facies code | Description | Average thickness | Accessory features | Interpretation |
|---|---|---|---|---|
| Gc | Clast-supported gravels | Tens of meters | Medium to coarse-grained sands as matrix | Competent tractional flows |
| Smg | Fine to very coarse-grained and massive sands | 20 cm to a few meters | Scattered pebbles or mud clasts overlying erosional surfaces | Strong tractional flows with multiple stages of erosion marked by pebble lags |
| Sm | Very fine to medium-grained and massive sands | 20 cm to a few meters | | |
| Sh | Fine-grained sands with horizontal laminations | 20–30 cm | | Upper flow regime tractional flows |
| Sx | Sands with cross laminations | 10–20 cm | | Dune or scour fills |
| SMh | Sands and muds interlayers with inclined heterolithic beddings | 5–20 cm | Flaser, wavy or lenticular beddings<br>Sand/mud ratio:<br>Flaser: 8:1–5:1<br>Lenticular: 1:3–1:5 | Alternating high and low energy conditions, probably tidal process |
| Mm | Massive muds and silts | 20 cm to a few meters | Sometimes with very fine laminations | Standing water body, abandoned channel, overbank, lake |
| Mfm | Fossiliferous massive muds and silts | 20 cm to a few meters | With abundant shell fragments and foraminifera | Brackish standing water body, lagoon, estuary |

**Table 3**
Facies association descriptions and interpretations for the upper Pleistocene to Holocene sediments in the Taipei Basin.

| Depositional system | Facies association code | Principal facies assemblage | Description | Sedimentary environment |
|---|---|---|---|---|
| Fluvial | GB | Gc | Grain size: small to large pebbles, composed of sub-rounded sandstones and meta-sandstones<br>Color: yellowish-brown sand matrix | Gravelly braided channel |
| | SB | Sm, Smg | Grain size: medium to very coarse sands with granules or small pebbles<br>Color: grey to yellowish-grey | Sandy braided channel |
| | CH | Sm, Smg, Sh, Sx | Grain size: fine to coarse-grained. Granules, small pebbles or mud clasts at base. Overall fining-upward to muds to very fine sands.<br>Color: grey to yellowish-grey<br>Sedimentary structures: horizontal and cross laminations, bioturbations<br>Accessories: plants remains, wood fragments | Meandering channel |
| | FL | Mm, Sh | Grain size: muds to silts<br>Color: grey, episodic yellowish-brown to reddish-brown<br>Sedimentary structure: horizontal laminations, bioturbations<br>Accessories: plant remains, wood fragments, carbonaceous materials, vivianites | Floodplain |
| Estuarine | CB | Mfm | Grain size: muds to silts<br>Color: grey to dark grey<br>Sedimentary structure: bioturbations<br>Accessories: carbonaceous materials<br>Fossils: abundant shell fragments and foraminifera | Central basin |
| | BD | Sm, Sh, Sx, SMh | Grain size: fine to coarse-grained sands<br>Color: grey, yellowish-brown<br>Sedimentary structures: horizontal and cross laminations, bioturbations, few flaser and wavy beddings<br>Accessories: plant remains, wood fragments<br>Fossils: shell fragments, few foraminifera | Bayhead delta |
| | TF | Mm, Sh, SMh | Grain size: mud to silts<br>Color: grey, yellowish-grey<br>Sedimentary structures: horizontal laminations, lenticular and wavy beddings, bioturbations<br>Accessories: plant remains, wood fragments, carbonaceous materials, vivianites<br>Fossils: shell fragments, foraminifera | Tidal flat |

Sungshan Fm (Fig. 5). The total thickness is 18 m in the northwestern part of the basin and decreases towards the south and southeast. It comprises fossiliferous, grey to dark grey, massive muds to silts (Mfm) with abundant carbonaceous materials; few plant remains and wood fragments (Fig. 7A). The most significant features are the presence of numerous shell fragments and a high diversity of foraminifera; both euryhaline, e.g. *A. beccarii* and *Elphidium* spp., and normal-salinity, e.g. *F. scaphum, Globigerina* spp., *S. globosa* and *Neoglobigerina* sp., foraminiferal species are noted in this facies association.

The appearance of normal-salinity foraminiferal species indicates that the CB environment had a free connection with the open sea, and the massive, structureless muds indicate a low-energy depositional environment. We therefore interpret that the CB facies association is characteristic of an estuarine central basin. It is worth mentioning that no tidal rhythmites have been observed; this may be due to very low tidal energy in the inland basin. This feature is similar to other low-energy estuaries, such as the Mono Estuary in Benin, Africa (Anthony et al., 1996), the Guadiana Estuary in Portugal (Boski et al., 2002) and the Parana Basin in Brazil (Holz, 2003).

## 5. Stratigraphic architecture

Fig. 8 shows two cross sections oriented along strike (Fig. 8A) and perpendicular (Fig. 8B) to the basin-bounding Sanchiao Fault. The

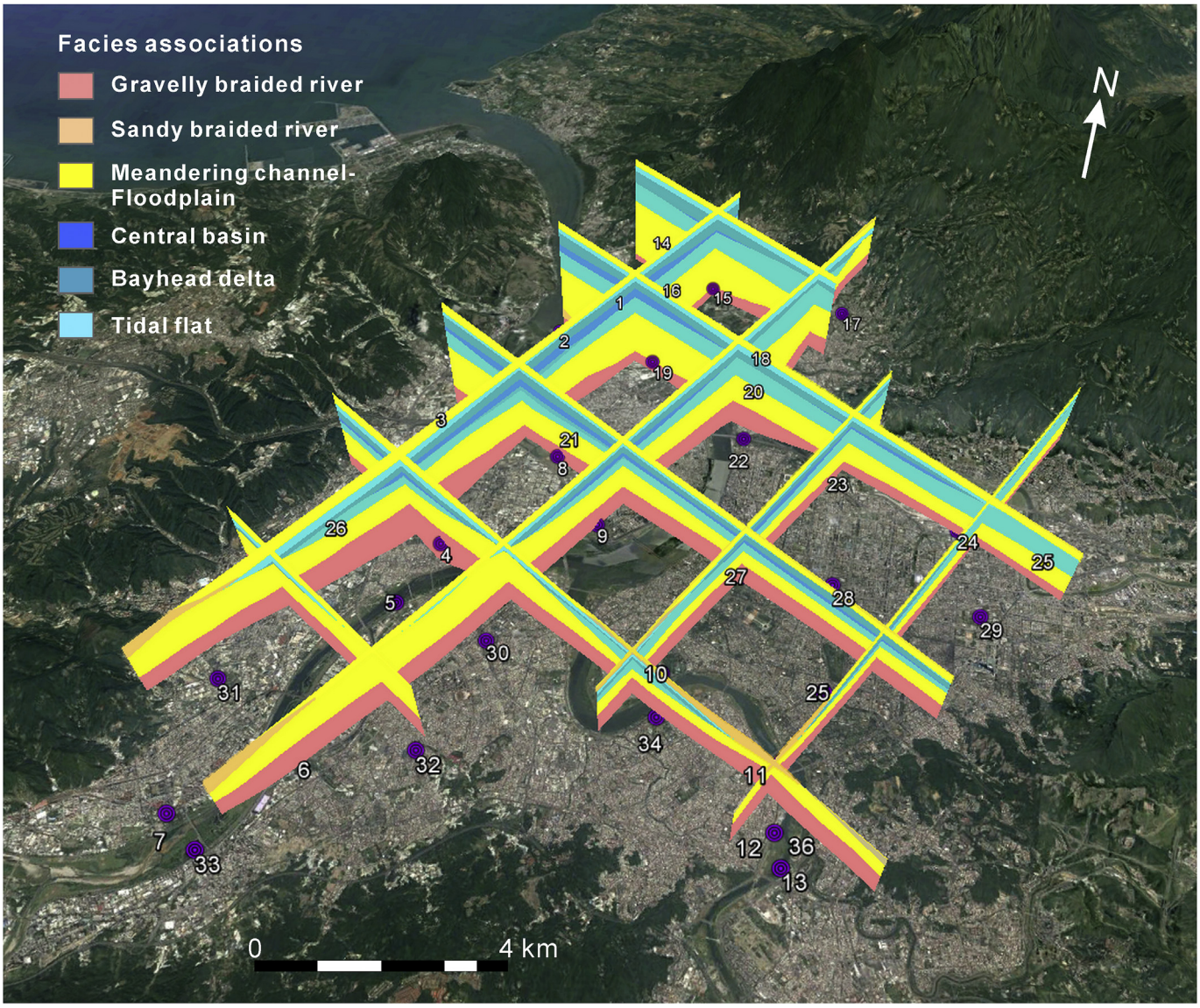


**Fig. 5.** Simplified 3D distribution model of the facies associations in the Taipei Basin. Vertical exaggeration is 25 times.

vertical fluvial–estuarine–fluvial stratal stacking pattern of the upper Pleistocene to Holocene Taipei Basin fill is similar to that proposed by wave-dominated models for late Quaternary estuaries on stable coasts (e.g. Dabrio et al., 2000; Amato et al., 2013). However, the layers thicken towards the bounding fault in the northwest part of the basin, exhibiting wedge-shaped stratal geometries. This wedge-shaped geometry, which is a characteristic feature of half grabens (Schlische, 1991; Bosence, 1998), is particularly evident in the lower part of the Sungshan Fm, consisting of meandering river facies.

The depositional age of the Jingmei Fm, i.e. between 50 ka and 20 ka, is constrained by several radiocarbon dating results from boreholes (nos. 2, 4, 21 and 22) as well as the ages of the underlying Wuku Fm and overlying Sungshan Fm (Su et al., 2016). The age of the basal Jingmei Fm appears to show a younging trend towards the distal basin margin, similar to the base of the Sungshan Fm (Figs. 8 and 9). In the northwest part of the basin, sediments of the Sungshan Fm started to accumulate 35 ka, which is 25 kyr earlier than the sediment accumulation in the southern and southeastern areas of the basin.

Previous studies (Teng et al., 2000; Chen et al., 2008) suggested that there is no unconformity/hiatus between the Jingmei Fm and the overlying Sungshan Fm. However, we argue that there is an unconformity/hiatus (approximately 11-kyr time gap) between these formations based on two observations: (1) the mud-rich meandering river facies of the Sungshan Fm abruptly overlie the gravel-rich braided river facies of the Jingmei Fm, implying a sedimentary discontinuity and (2) borehole correlations show that various isochronous surfaces of the lower Sungshan Fm progressively onlap onto the Jingmei Fm (Fig. 8).

In the southeastern part of the basin, the estuarine muds are erosively overlain by sandy braided river facies, e.g. boreholes 10 and 11 (Fig. 9), indicating the existence of another hiatus. High-resolution radiocarbon age constraints from borehole no. 10 indicate an approximately 4-kyr time gap in the sedimentary record spanning from 8 ka to 4 ka.

In the proximal basin area near the Sanchiao Fault, vertical changes in sedimentary facies are gradual and no major erosional surfaces are observed, e.g. borehole nos. 1 and 2 (Fig. 8).

## 6. Discussion

### 6.1. Basin subsidence

The stratigraphic and palaeoenvironmental framework for the Taipei Basin during the past 50 kyr is established in this study. We then

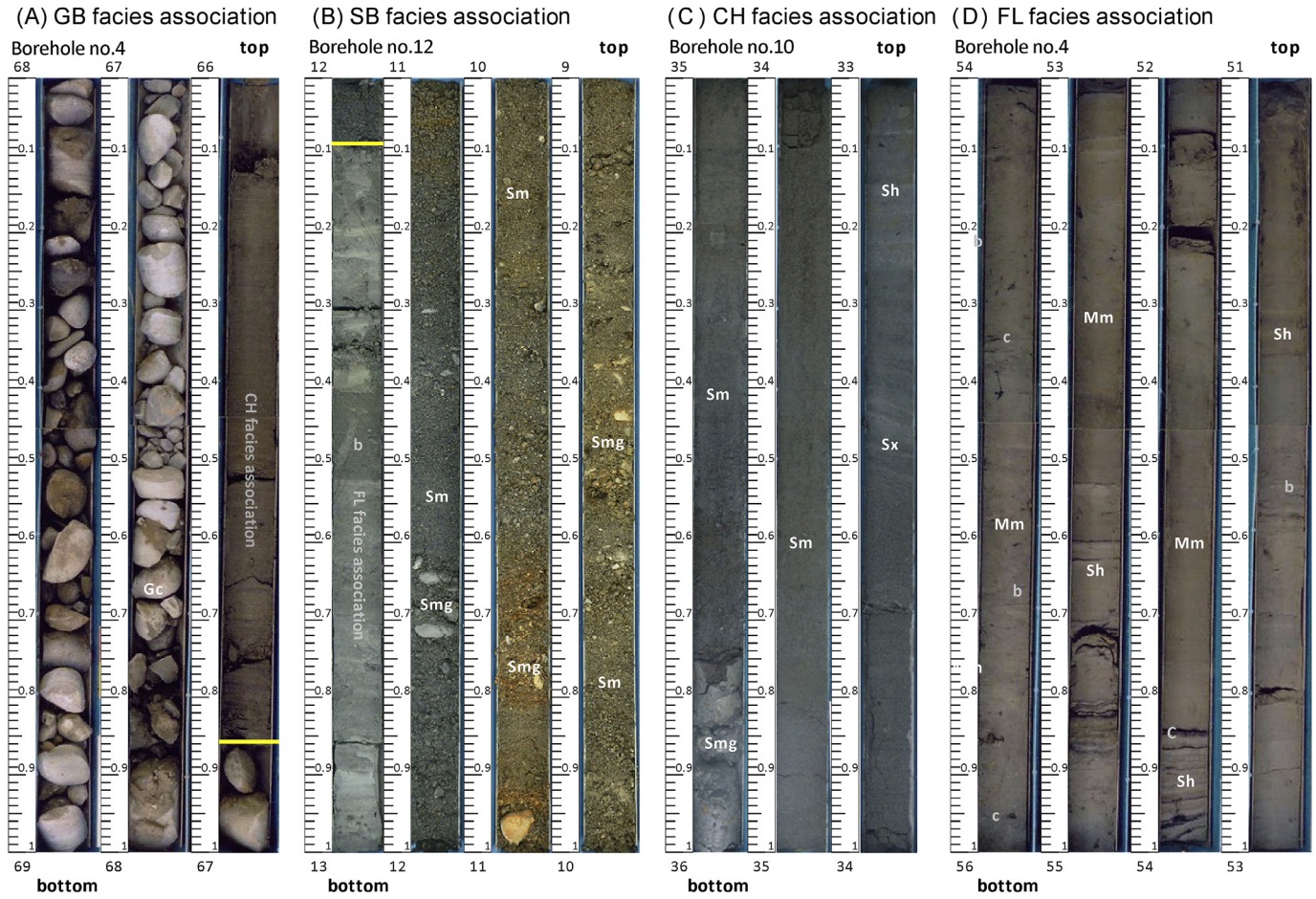


**Fig. 6.** Core photographs showing the fluvial facies associations. (A) GB (gravelly braided river) facies association, (B) SB (sandy braided river) facies association, (C) CH (meandering channel) facies association and (D) FL (floodplain) facies association. Lithofacies constituting each facies association are denoted by combinations of letters (Gc, Sm, etc.) and their acronym definitions and descriptions can be found in Table 2. c: carbonaceous material, b: bioturbation, s: shell fragments. Scale is in metres.

consider the spatiotemporal variations in basin subsidence using a modified backstripping method. Periodic basin subsidence can be deciphered as changes in sample depth over time, with known present-day sampled depth, palaeowater depth and height of eustatic sea level, using the following formula:

$$T_{[n-(n+1)]} = (\Delta S_{n+1} + D_{n+1}) - (\Delta S_n + D_n) + (H_n - H_{n+1})$$

Fig. 10 shows all of the parameters used in the formula. T represents the change in sample elevation, regarded as basin subsidence, $\Delta S$ represents the height of eustatic sea level compared with that in the present day, D represents the water depth at the time of deposition and H represents the sampled depth below the present-day sea level. We adopted the eustatic curve for the past 21 kyr from Chen and Liu (1996), Hanebuth et al. (2000) and Bird et al. (2007), which Hsieh et al. (2006, 2016) suggested to be applicable in the Taiwan region; eustatic sea level prior to 21 ka is from Waelbroeck et al. (2002). The studied succession is limited to the upper 140 m beneath the ground surface; at this interval, sediment compaction is considered negligible and is not included in the calculation. Of the above parameters ($\Delta S$, D and H), palaeowater depth (D) needs to be carefully determined because the amount of basin subsidence is sensitive to it. Palaeowater depths are deduced from the palaeoenvironments (estuarine central basin, tidal flat/bayhead delta, floodplain, meandering channel and braided river), from deeper water to subaerial and proximal settings. However, it is difficult to determine the precise palaeoenvironmental elevations, particularly for the terrestrial environments (e.g. braided river).

To better constrain palaeowater depths, we use the temporal height difference between the relative sea level (RSL) curve and the sediment accumulation curve, following the method employed by Tanabe et al. (2013). Considering borehole no. 2 as an example (Fig. 11), the sediment accumulation curve is plotted from the dated horizons at the sampled depths, and the RSL curve is derived from the eustatic sea level curve with an additional, uniform basin-subsidence rate. For this, a reasonable basin-subsidence rate that explains the palaeoenvironments and palaeowater depths is required. We determine the uniform basin-subsidence rate by two approaches: (1) previous basin subsidence studies for the Taipei Basin, as shown in Table 4, from which the suggested rates of basin subsidence during the past 40 kyr are 0.7–2.4 mm/yr, and (2) trial-and-error analysis using the above range of basin subsidence rates to obtain the RSL curve and the resultant palaeowater depths. Comparing the derived palaeowater depths (dashed green line in Fig. 11) and the palaeoenvironments indicated by the sedimentary facies shows that a uniform basin-subsidence rate of 1.75 mm/yr 40 ka best matches the palaeoenvironments at the location of borehole no. 2. The derived palaeowater depths fit the sedimentary facies, with the elevations of the braided river and meandering river facies approximately 20–40 m above RSL at the time of deposition and the estuarine central basin facies a few meters below RSL. However, there is a mismatch with respect to the floodplain facies; the derived palaeowater depths indicate deposition at a water depth of up to 9 m, although the facies are interpreted as a subaerial floodplain facies. There is also a mismatch of a few metres between the derived palaeowater depths and inferred palaeoenvironments for the estuarine facies. The water-depth discrepancy could result from mud compaction, because mud is the

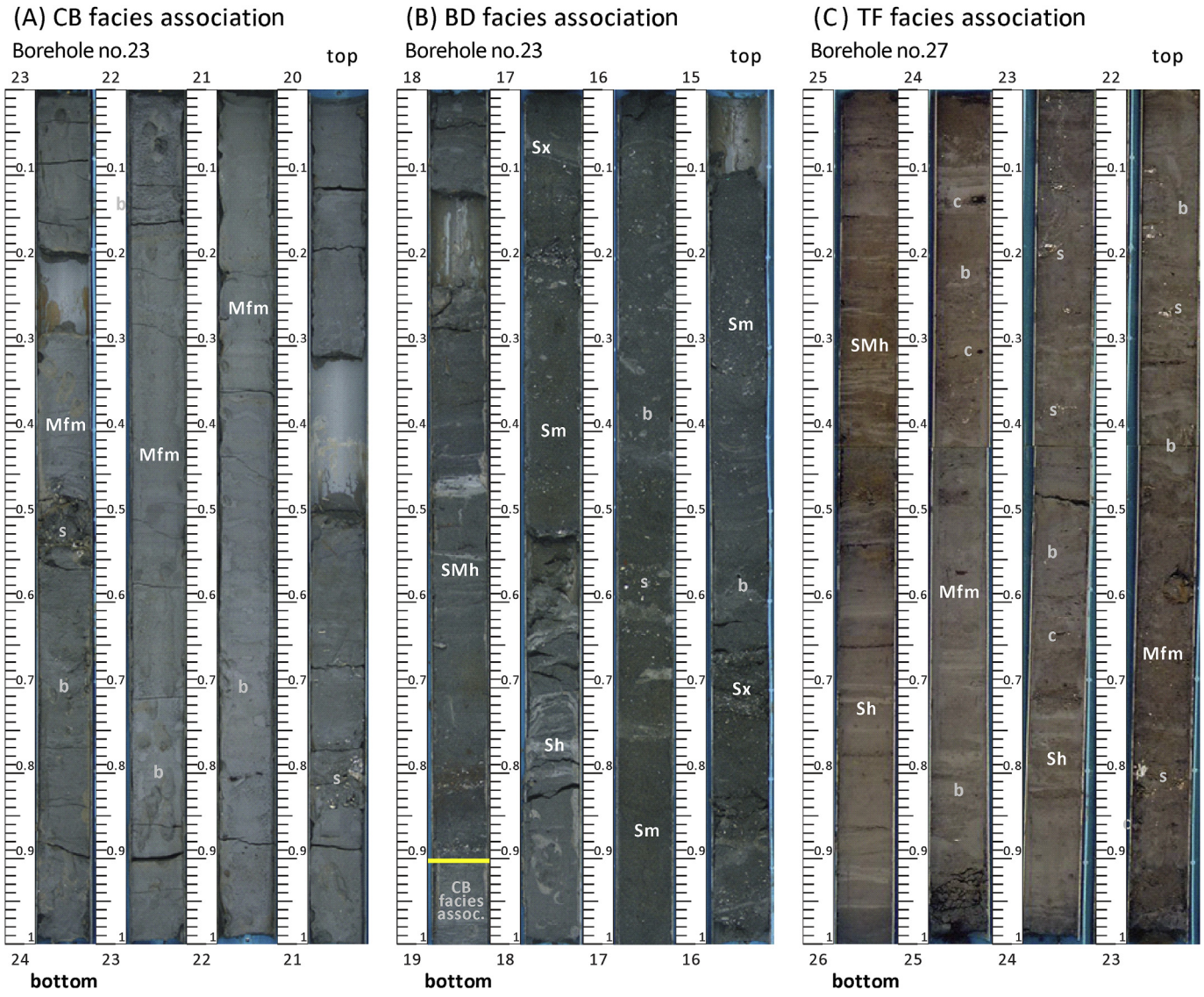


**Fig. 7.** Core photographs showing the estuarine facies associations. (A) CB (central basin) facies association, (B) BD (bayhead delta) facies association and (C) TF (tidal flat) facies association. All scales, abbreviations and symbols are the same as in Fig. 6. The lithofacies acronym definitions (SMh, Mfm, etc.) and descriptions can also be found in Table 2.

predominant lithology for the studied interval consisting of floodplain, estuarine tidal flat and central basin facies. To account for the sedimentary facies, we manually adjust the palaeowater depths or elevations for the floodplain/bayhead delta/tidal flat/central basin facies with reference to modern settings, and the adjusted curve is shown as a solid green line in Fig. 11. The mismatches between the derived palaeowater depths and the sedimentary facies between ~12 ka and 6 ka indicate that the rate of basin subsidence during this period cannot be explained by a uniform subsidence. Similar calculations were also applied to borehole nos. 3, 4, 5, 10 and 27. The results show that a lower, uniform subsidence rate of approximately 1.5–1.0 mm/yr in the distal fault area yields good matches between the inferred palaeowater depths/elevations and the sedimentary facies.

The reliability of the basin subsidence curve is determined by the amount and spacing of the age dates. Borehole nos. 2, 3, 4 and 5, located in the proximal fault area, were selected for examining basin subsidence because the depositional records are relatively continuous with abundant dated datum levels. Borehole nos. 10 and 27, located in the distal fault area, were also selected for comparison. Table 5 lists all the calculated stratigraphic horizons with the various parameters for the studied boreholes, and Fig. 12 shows the basin subsidence curves. We note that changes in the basin subsidence rate can only occur at the dated horizons and that these points of change may not reflect the exact time when the rate of subsidence varied. The consistent general trend for all the boreholes shown in Fig. 12 indicates that our data and analyses are robust.

The subsidence curves show two likely episodes of rapid basin subsidence, which occurred between ~11 ka and 8 ka, superimposed on a period of uniform subsidence rates of ~1.0–1.75 mm/yr. The durations of the two phases of rapid basin subsidence can be constrained using overlapping time spans with 95% confidence intervals (2-σ) of age dates, which are plotted in Fig. 13. The first rapid basin-subsidence episode, which occurred between ~10.6 ka and 10.2 ka, was recorded in borehole nos. 2 and 3, whereas the second phase, which occurred between ~9 ka and 8.5 ka, was recorded across a wider area.

Similar results have been reported by Huang et al. (2007) and Chen et al. (2010a). Chen et al. (2010a) used a stratigraphic profile across the Sanchiao Fault to compare the differences in layer thickness between the hanging wall and footwall and observed that a rapid phase of basin subsidence occurred 9–8.4 ka. Owing to a lack of age dates between 23 ka and 9 ka, Chen et al. (2010a) did not detect the rapid basin-

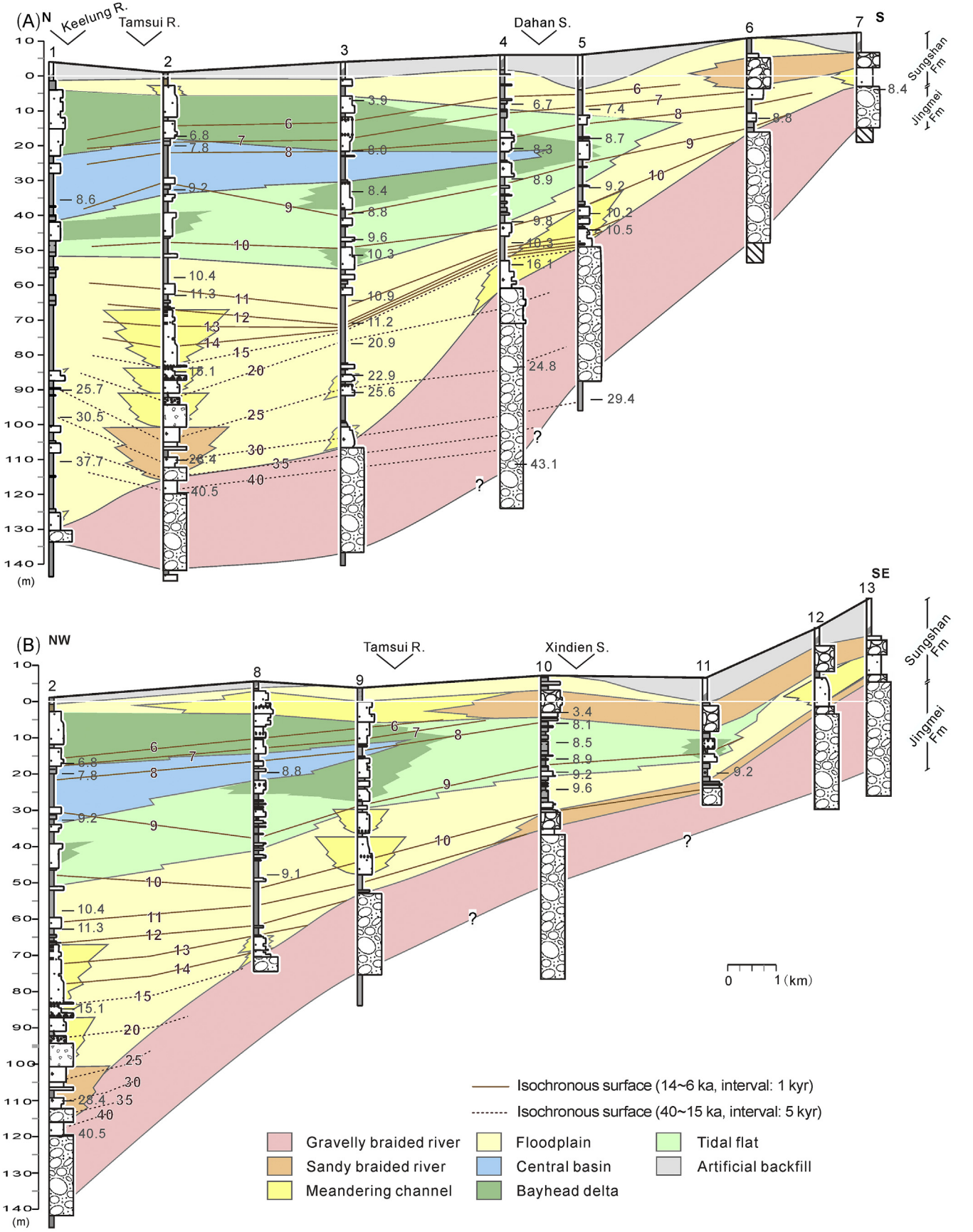


**Fig. 8.** Facies association distributions and isochronous surfaces for cross section 1 (A) and cross section 2 (B). Cross section locations are shown in Fig. 1B. Lithology patterns of the borehole sedimentological columns are the same as in Fig. 3. Radiocarbon ages are expressed as median values in ka. Reworked or unreliable age dates are not shown here. Note that the isochronous surface interval is 5 kyr for the ages spanning 40–15 ka and 1 kyr for those spanning 14–6 ka.

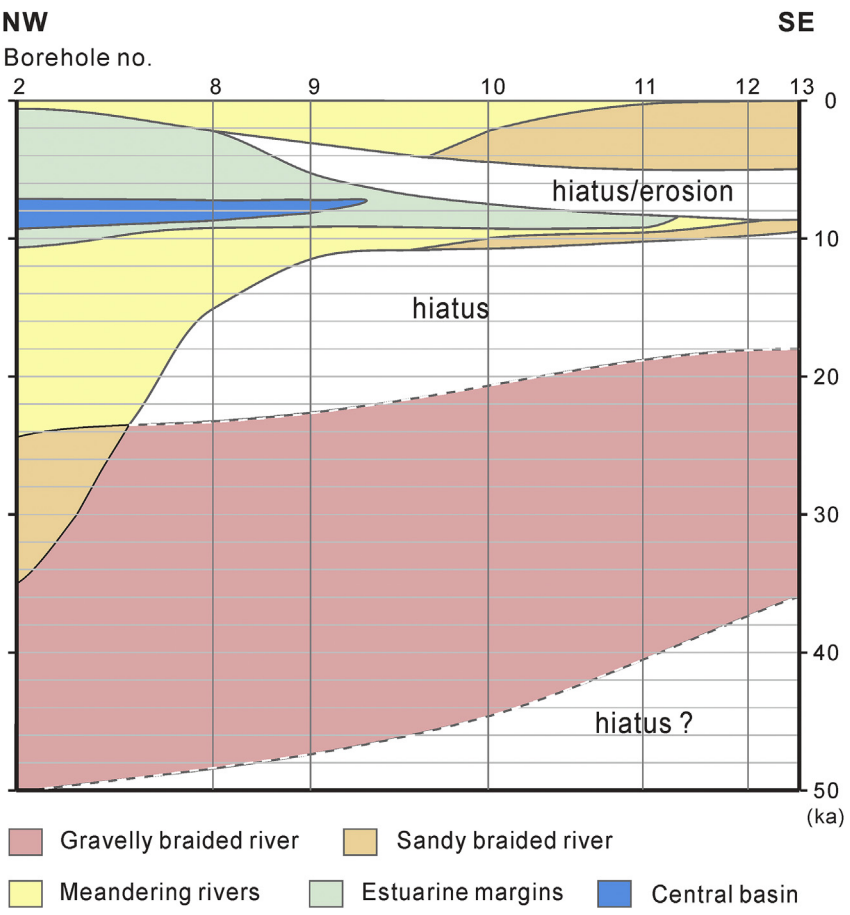


**Fig. 9.** Chronostratigraphic chart based on the NW–SE-oriented cross section 2 shown in Fig. 8B denoting the spatio-temporal distribution of palaeoenvironments and stratigraphic hiatuses. Regarding palaeoenvironments, tidal flats and bayhead deltas are combined as estuarine margins, and meandering channels and floodplains are combined as meandering rivers.

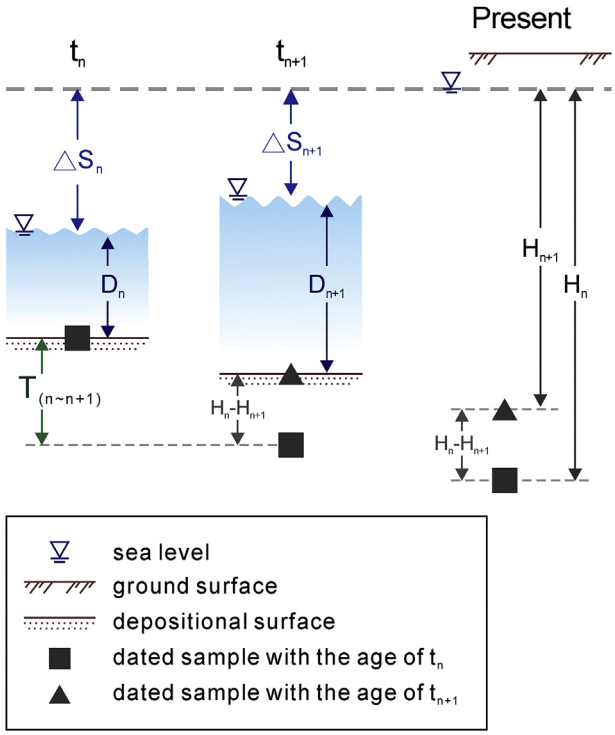


**Fig. 10.** Illustration of calculations of basin subsidence magnitude through time. D: water depth at the time of deposition, H: present-day sample depth referenced to sea level, S: height of sea level with reference to present-day sea level, T: amount of subsidence, t: age.

subsidence phase 10.6–10.2 ka, as reported in this study. Huang et al. (2007) compared the elevation differences of key beds in the Sanchiao Fault Zone and suggested that three palaeoearthquakes occurred approximately 11.1 ka, 9–9.3 ka and 8.6–8.4 ka. There are notable time differences between the earthquake events reported by Huang et al. (2007) and the rapid-subsidence phases reported in this study, which may arise from different dated horizons.

### 6.2. *Tectonic controls on stratigraphic development*

The stratigraphic development of the Taipei Basin during the past 50 kyr is described in detail in Section 5. The studied chronostratigraphy is shown in Fig. 9 and is discussed for two locations. These are 1) the proximal fault area, where sedimentation is strongly controlled by normal faulting and eustatic sea level changes, as well as sediment supply and 2) the distal fault area, which shows two stratigraphic hiatuses.

In the proximal fault area, illustrated here using borehole no. 2 (Figs. 3, 8 and 9), during eustatic sea level fall ~50–35 ka, the depositional environment was characterised by gravelly braided rivers. While eustatic sea level fell rapidly by approximately 40 m between ~35 ka and 20 ka during the Marine Isotope Stage (MIS) 3/2 transition, reaching the lowest level, the depositional environment changed from gravelly braided rivers, through sandy braided rivers to meandering rivers, including meandering channels and floodplains, with sediment thickness of up to ~20 m in the proximal fault area. This temporal facies change reflects an RSL rise (e.g. Törnqvist, 1993; Blum and Törnqvist, 2000; Tanabe et al., 2015) instead of a falling sea level. However, there are several plausible explanations for this observation.

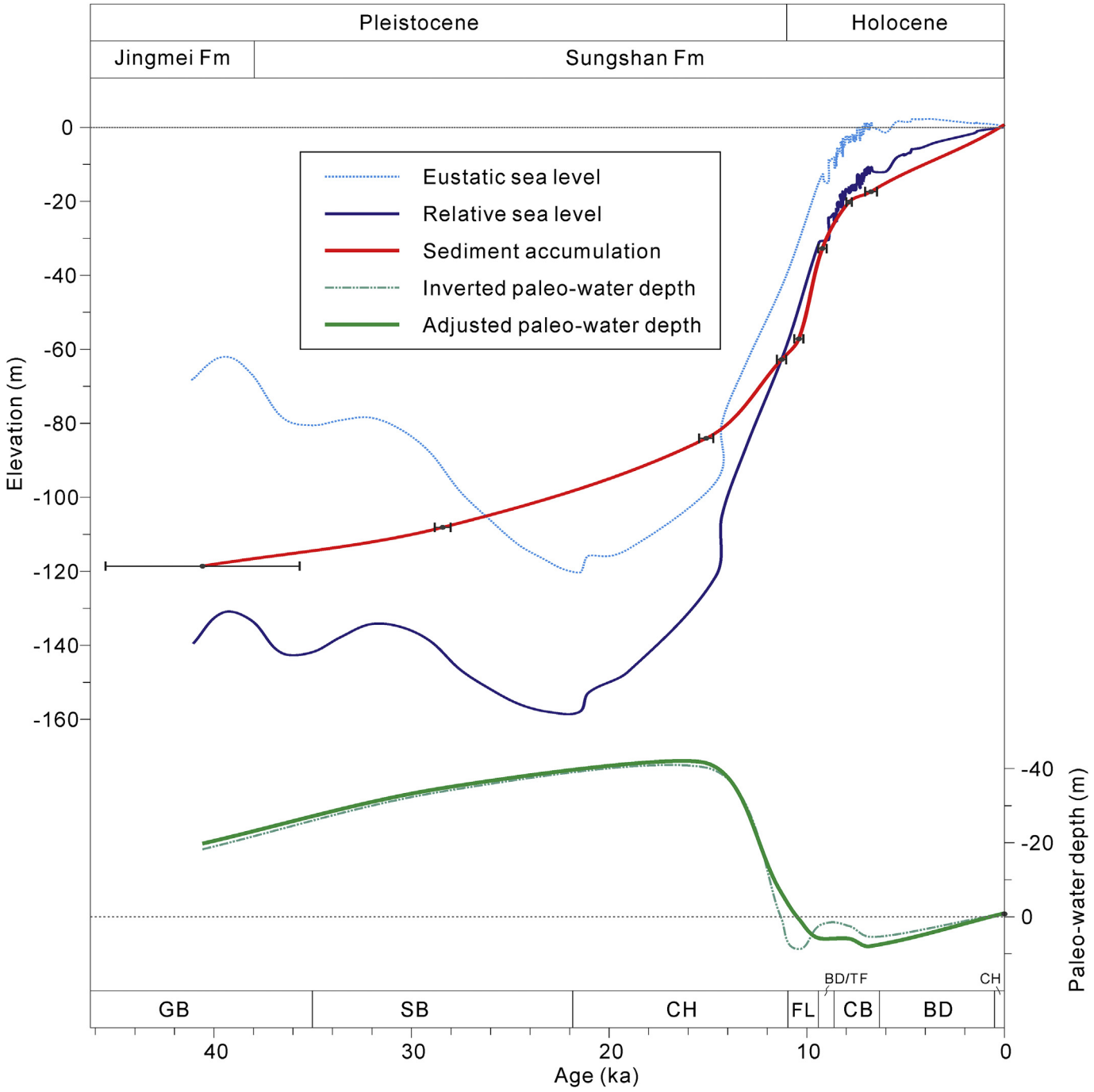


**Fig. 11.** Comparison of eustatic sea levels (Chen and Liu, 1996; Hanebuth et al., 2000; Waelbroeck et al., 2002; Bird et al., 2007) and sediment accumulation curves for borehole no. 2. Relative sea level (RSL) represents the sea level height (with reference to present-day sea level) assuming a constant basin-subsidence rate of 1.75 mm/yr. The difference between the RSL and the sediment accumulation curves is the inverted palaeowater depth. The adjusted palaeowater depths are manually tuned where the inverted palaeowater depths are unreasonable by reference to the facies associations and analogy with water depths in modern environments. The abbreviations of facies associations and descriptions can be found in Table 3 and in text.

During this period, the rate of basin subsidence may have outpaced the combined rates of eustatic sea level fall at ~2.67 mm/yr and sediment supply, which should be on the order of a few mm per year according to reported erosion rates for the Taiwan mountain belt in the late Quaternary (e.g. Dadson et al., 2003). It is possible that there was a higher rate of basin subsidence between ~35 ka and 20 ka, though this high value far exceeds the reported rates of basin subsidence (0.7–2.4 mm/yr) in the late Quaternary (Table 4). Another possible explanation is that the temporal facies change from gravelly braided rivers to meandering rivers between 35 ka and 20 ka resulted from a decrease in river

**Table 4**
List of basin subsidence rates for the past 400 kyr in the Taipei Basin from published reports.

| References | Basin subsidence rates (mm/yr) | Materials & methods |
|---|---|---|
| Wei et al. (1998) | 1.2–2.1 (after 220 ka)<br>1.1–2.4 (after 90 ka) | Comparison of eustatic sea levels, age datings, and sampled depths from borehole no. 3. |
| Huang et al. (2007) | 2.25 (after 400 ka)<br>0.69 (after 15 ka)<br>1.8 (after 10 ka) | Comparison of sampled depths and corresponding age datings from boreholes in the Sanchiao fault zone. |
| Chen et al. (2008) | 1.2 (after 400 ka)<br>1.2–1.5 (Holocene) | Comparing climates from pollen occurrences and sedimentary environments mainly from borehole no. 3. |
| Chen et al. (2010a) | 1.1–2.2 (after 23 ka)[a]<br>0.9–2.3 (after 8.4 ka) | Comparing the difference of layer thickness from boreholes drilled in the footwall and hanging wall of the Sanchiao fault (near borehole no. 3). |

[a] The dating of 23 ka from the bottom of borehole no. 2 should be calibrated to 28 ka so the tectonic subsidence rates become 0.9–1.8 mm/yr.

gradients, which may have been caused by a decrease in flow competence due to drier climates, as seen in other river systems worldwide after 30 ka (Fuller et al., 1998; Blum et al., 2000; Dabrio et al., 2000; Maddy et al., 2001; Ta et al., 2002; Bhandari et al., 2005; Amorosi et al., 2012).

During the deglacial period and rising eustatic sea level between ~20 ka and 6 ka, the palaeoenvironment changed from meandering rivers to estuary in the proximal fault area, with sediment layers reaching up to 80 m in thickness (Figs. 3, 8 and 9). The deepest estuarine environment developed ~8 ka when the eustatic sea level was ~5 m below the present-day sea level. During the past 6 kyr, the proximal fault area was gradually infilled to produce the meandering river environment of the present day.

The thickness of the meandering river sediments (~20–10.2 ka in age) is ~40 m and is much greater than their depositional depth, which is nearly zero. This implies an increase in accommodation space and sediment supply, as similarly discussed for other study areas (e.g. Muto and Steel, 1997; Goodbred and Kuehl, 2000; Muto and Steel, 2002; Tanabe et al., 2013).

Two episodes of rapid basin subsidence, ~10.6–10.2 ka and ~9–8.5 ka, are described in Section 6.1. The first rapid basin-subsidence phase resulted in a palaeoenvironment change from meandering rivers to estuarine margins, i.e. tidal flats and bayhead deltas, and the latter phase is recorded in estuarine facies in the Taipei Basin (Fig. 13). The first brackish estuarine facies was deposited ~10.2 ka. Similarly, estuarine facies occurred in central Taiwan ~15–10 ka (Chen et al., 2010b) and in southern Taiwan ~10 ka (Hsieh et al., 2006). The nearly coeval existence of the estuarine facies in northern (this study), central (Chen et al., 2010b) and southern (Hsieh et al., 2006) Taiwan indicates that the eustatic sea level rise is the predominant control for environmental change from fluvial to estuarine. Additionally, the rapid rise of sea level (> 13 m/kyr) around 11–10 ka in Taiwan (Hsieh et al., 2006), which corresponds to the period of meltwater pulse 1B (e.g. Fairbanks, 1989; Liu and Milliman, 2004; Bard et al., 2010), may have promoted the early appearance of an estuary. A study on the Italian Po Plain (Bruno et al., 2017) suggests that rapid eustatic sea level rises promote shoreline transgressions and the occurrence of coastal facies. These phenomena attest that the rapid eustatic sea level rise was the dominant control for the appearance of the first estuarine facies in the active subsiding Taipei Basin and that rapid basin subsidence modulated the accommodation space in the inland basin. The 2–3 kyr earlier onset of the brackish environments in the Taipei Basin than other Holocene coastal estuaries, which first appeared ~8–7 ka (Heap and Nichol, 1997; Nichol et al., 1997; Amorosi et al., 1999, 2008; Abrahim et al., 2008; Bastos et al., 2010; Sloss et al., 2010; Fornari et al., 2012), might be due to their different lateral positions in the estuaries.

The second rapid basin-subsidence phase (~9–8.5 ka) is recorded, as a minimum, in borehole nos. 3, 4, 5, 10 and 27. Estuarine deposits were widespread in this phase, while the meandering and sandy braided river deposits were only distributed around the basin margin (Fig. 13). Additionally, there is an age discrepancy between the deepest palaeowater depths (i.e. central basin estuarine facies occurring ~9–8 ka) and the highest eustatic sea level (~5 ka). The coeval minor rapid sea level rise (Leorri et al., 2013; Tanabe et al., 2015; Bruno et al., 2017) may have widened the estuary, similar to the mechanism for the first estuarine deposits in the basin, and the basin subsidence may have been the subsidiary controlling factor.

After ~7 ka, an overall shallowing-upward trend is observed in the proximal fault area. During this time, the estuarine systems began to retreat from the basin, and the basin was finally infilled by meandering channel and floodplain deposits similar to those of the present day. Furthermore, during the past 6 kyr, the eustatic sea level was nearly stable and the nominal rate of basin subsidence was also constant (Fig. 12); hence, the shallowing and progressive infilling of the basin was due to a higher rate of sediment supply rather than basin subsidence. Therefore, in our case, the nominal sediment-supply rate for the past 6 kyr should be higher than ~1.75 mm/yr.

In the distal fault area, the temporal palaeoenvironmental development trend is similar to that of the proximal fault area, except for two episodes of hiatus—one between ~22 ka and 11 ka and the other between ~8 ka and 4 ka—as described in Section 5 and shown in Fig. 9. These hiatuses are due to erosion or lack of accommodation space available for sediment accumulation. In a typical half graben, such as the Taipei Basin, the amount of basin subsidence decreases towards the distal fault basin margin, as shown in many other studies (e.g. Doglioni et al., 1998). The hiatuses in the Taipei Basin indicate that no accommodation space was available for deposition and that fluvial sediments simply bypassed the basin margin during those periods.

## 7. Conclusions

The late Quaternary (< 50 ka) stratigraphy of the Taipei Basin shows a vertical fluvial–estuarine–fluvial stacking pattern representing a complete retrogradational to progradational sedimentary cycle. However, the temporal changes in the palaeoenvironment do not always coincide with the corresponding eustatic fluctuations. Our basin subsidence analyses indicate that basin subsidence and sediment supply were essential in shaping the studied stratigraphy of the Taipei Basin, though eustatic sea level changes were the dominant control for basin stratigraphy.

**Table 5**
List of parameters for borehole nos. 2, 3, 4, 5, 10 and 27 used to calculate the amount and rates of basin subsidence during the past 50 kyr. Palaeoenvironment abbreviations are described in text and in Table 3.

| Borehole | Sampled depths, H (m) | Median age, t (cal BP) | Eustatic sea level, △S (m) | Environments & paleo water depth, D (m) | | Amount of subsidence, T (m) | Basin subsidence rate, R[a] (mm/yr) |
|---|---|---|---|---|---|---|---|
| 2 (Ground level: 1.001m) | −1.0 | 0 | 0 | FL | −1.0 | −9.3 | −1.4 |
| | 17.3 | 6800 | 0.0 | BD | 8.0 | −0.9 | −0.8 |
| | 20.2 | 7840 | −4.1 | CB | 6.0 | −2.0 | −1.4 |
| | 32.8 | 9243 | −14.6 | CB | 6.0 | −14.2 | −12.6 |
| | 57.1 | 10368 | −30.3 | FL | 0.5 | −0.2 | −0.2 |
| | 62.8 | 11290 | −43.3 | FL | −7.0 | −1.5 | −0.4 |
| | 84.1 | 15110 | −98.1 | CH | −42.0 | −22.7 | −1.7 |
| | 108.1 | 28381 | −92.4 | SB | −35.0 | −21.9 | −1.8 |
| | 118.6 | 40509 | −66.0 | GB | −20.0 | – | – |
| 3 (Ground level: 3.971 m) | 3.97 | 0 | 0.0 | CH | −4.0 | −7.3 | −1.9 |
| | −6.23 | 3922 | 2.1 | CH | 1.0 | −4.5 | −1.1 |
| | −20.83 | 7983 | −3.0 | BD | 6.0 | −2.3 | −6.0 |
| | −32.58 | 8370 | −6.0 | BD | 12.5 | −5.3 | −12.9 |
| | −38.23 | 8782 | −8.8 | BD | 10.0 | −0.7 | −0.8 |
| | −46.33 | 9646 | −19.2 | TF | 7.0 | −0.3 | −0.5 |
| | −50.88 | 10249 | −28.5 | BD | 2.0 | −4.7 | −7.5 |
| | −63.68 | 10873 | −38.0 | FL | 0.5 | −1.2 | −3.3 |
| | −70.43 | 11230 | −42.6 | FL | 1.5 | −9.3 | −1.0 |
| | −76.53 | 20968 | −116.0 | FL | −75.0 | −1.9 | −1.0 |
| | −85.43 | 22872 | −117.9 | CH | −70.0 | −4.7 | −1.7 |
| | −90.08 | 25623 | −107.9 | CH | −60.0 | – | – |
| 4 (Ground level: 6.007 m) | 6.01 | 0 | 0.0 | CH | −6 | −7.6 | −1.1 |
| | −8.14 | 6720 | 0.4 | TF | 1.0 | −2.3 | −1.5 |
| | −20.89 | 8279 | −6.0 | BD | 5.0 | −5.8 | −9.7 |
| | −29.59 | 8875 | −9.9 | TF | 4.0 | −1.9 | −2.0 |
| | −41.84 | 9845 | −22.2 | TF | 2.0 | −0.9 | −2.1 |
| | −47.87 | 10275 | −28.9 | FL | 0.5 | −3.6 | −0.6 |
| | −54.19 | 16087 | −102.1 | CH | −70.0 | −9.3 | −1.1 |
| | −82.89 | 24832 | −111.5 | GB | −60.0 | −20.4 | −1.1 |
| | −111.09 | 43054 | −74.3 | GB | −15.0 | – | – |
| 5 (Ground level: 6.222 m) | 6.22 | 0 | 0.0 | | −6.2 | −7.8 | −1.1 |
| | −9.53 | 7417 | 0.2 | FL | 2.0 | −0.8 | −0.6 |
| | −18.03 | 8699 | −8.5 | TF | 1.0 | −8.1 | −17.8 |
| | −32.28 | 9151 | −14.6 | FL | 1.0 | −1.1 | −1.0 |
| | −39.33 | 10195 | −27.6 | CH | −6.0 | −0.3 | −1.0 |
| | −44.03 | 10451 | −31.6 | CH | −5.5 | −28.2 | −1.5 |
| | −92.63 | 29369 | −86.5 | GB | −40.0 | −31.5 | −1.7 |
| | −111.38 | 48008 | −73.7 | GB | −40.0 | – | – |
| 10 (Ground level: 11.1 m) | 11.10 | 0 | 0.0 | CH | −11.0 | −5.8 | −1.7 |
| | −0.59 | 3439 | 2.1 | SB | −3.0 | 8.2 | 1.8[b] |
| | −3.65 | 8101 | −5.2 | TF | 1.0 | −0.7 | −1.8 |
| | −8.93 | 8487 | −8.8 | TF | 2.0 | −2.6 | −6.5 |
| | −13.45 | 8892 | −11.7 | TF | 1.0 | −0.7 | −2.2 |
| | −17.07 | 9212 | −14.6 | FL | 1.0 | −0.3 | −0.8 |
| | −20.60 | 9561 | −17.9 | FL | 1.0 | – | – |
| 27 (Ground level: 4.983 m) | 4.98 | 0 | 0.0 | FL | | −7.9 | −1.4 |
| | −0.82 | 5823 | 1.1 | FL | −1.0 | −2.6 | −1.9 |
| | −6.52 | 7192 | −0.5 | FL | 0.5 | −0.4 | −0.4 |
| | −13.52 | 8319 | −6.6 | TF | 1.0 | −3.8 | −10.1 |
| | −19.17 | 8696 | −8.4 | TF | 1.0 | −0.3 | −0.3 |
| | −29.62 | 9867 | −22.6 | CH | −3.0 | −0.3 | −0.8 |
| | −35.32 | 10219 | −28.0 | FL | −3.0 | −0.3 | −0.9 |
| | −41.52 | 10569 | −33.4 | SB | −2.5 | – | – |

[a] $R = T_{(n+1\sim n)}/(t_{n+1}\text{-}t_n)$.
[b] The positive tectonic movement rate result in borehole no. 10 is resulted from the lack of sediments eroded by sandy braided river.

Combined with rapid sea level rise, the initial rapid basin-subsidence phase occurred between 10.6 ka and 10.2 ka, leading to the appearance of estuarine environments, and a second rapid basin-subsidence phase between 9.0 ka and 8.5 ka promoted widespread estuarine facies distribution. When the rate of basin subsidence remained relatively steady (in our case, 1.75 mm/yr), temporal palaeoenvironmental changes were controlled by changing rates of sediment supply. For example, a speculated low rate of sediment supply resulting from low flow competence between 35 ka and 20 ka led to a facies change from gravelly braided river to meandering river during the eustatic sea level fall; however, this could be because of rapid basin subsidence. Thick meandering river deposits accumulated in the basin between 20 ka and 10.2 ka when the sediment supply rates and eustatic sea level rise were balanced. Since 7 ka, the rate of basin subsidence has remained stable (i.e. 1.75 mm/yr) coupled with no eustatic fluctuations. As a result, the rate of sediment supply has become increasingly important and the depositional environment has changed from estuary to tidally influenced meandering rivers.

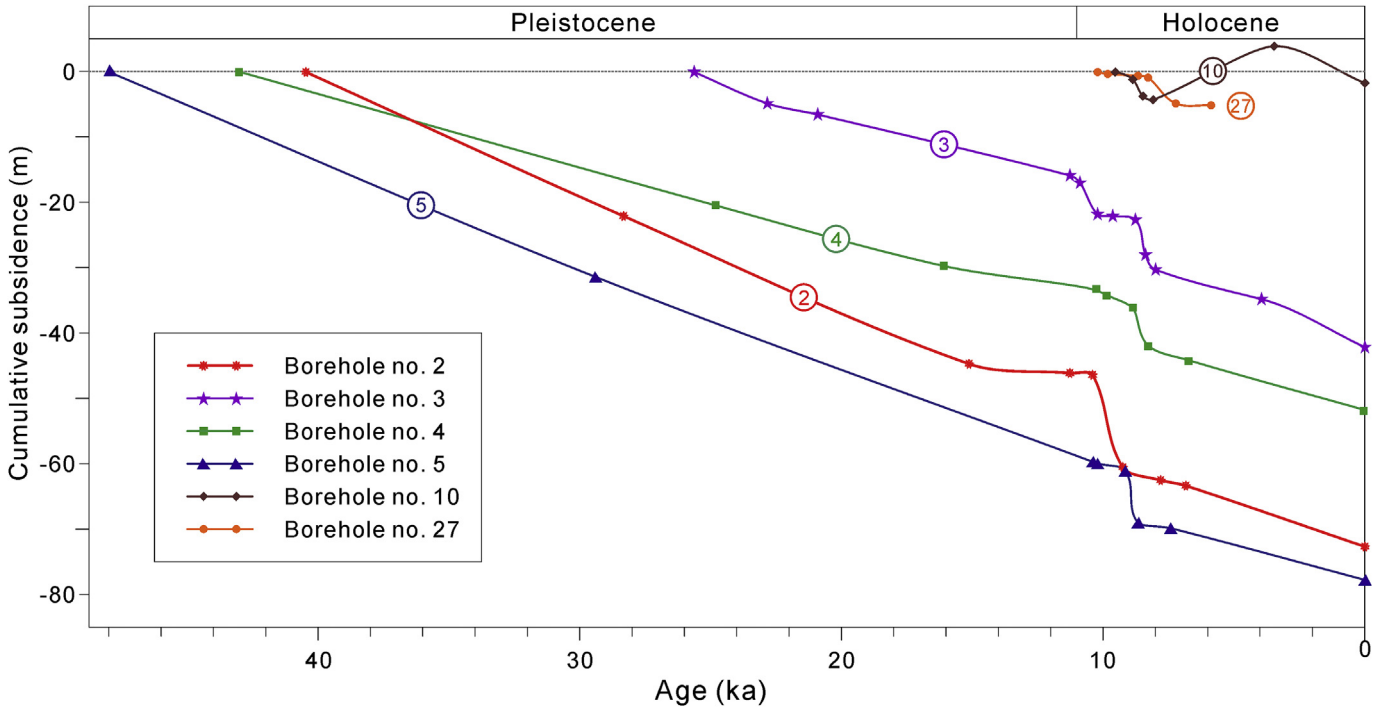


**Fig. 12.** Basin subsidence curves for selected boreholes representing various locations in the Taipei Basin during the past 50 kyr. See Fig. 1B for borehole locations.

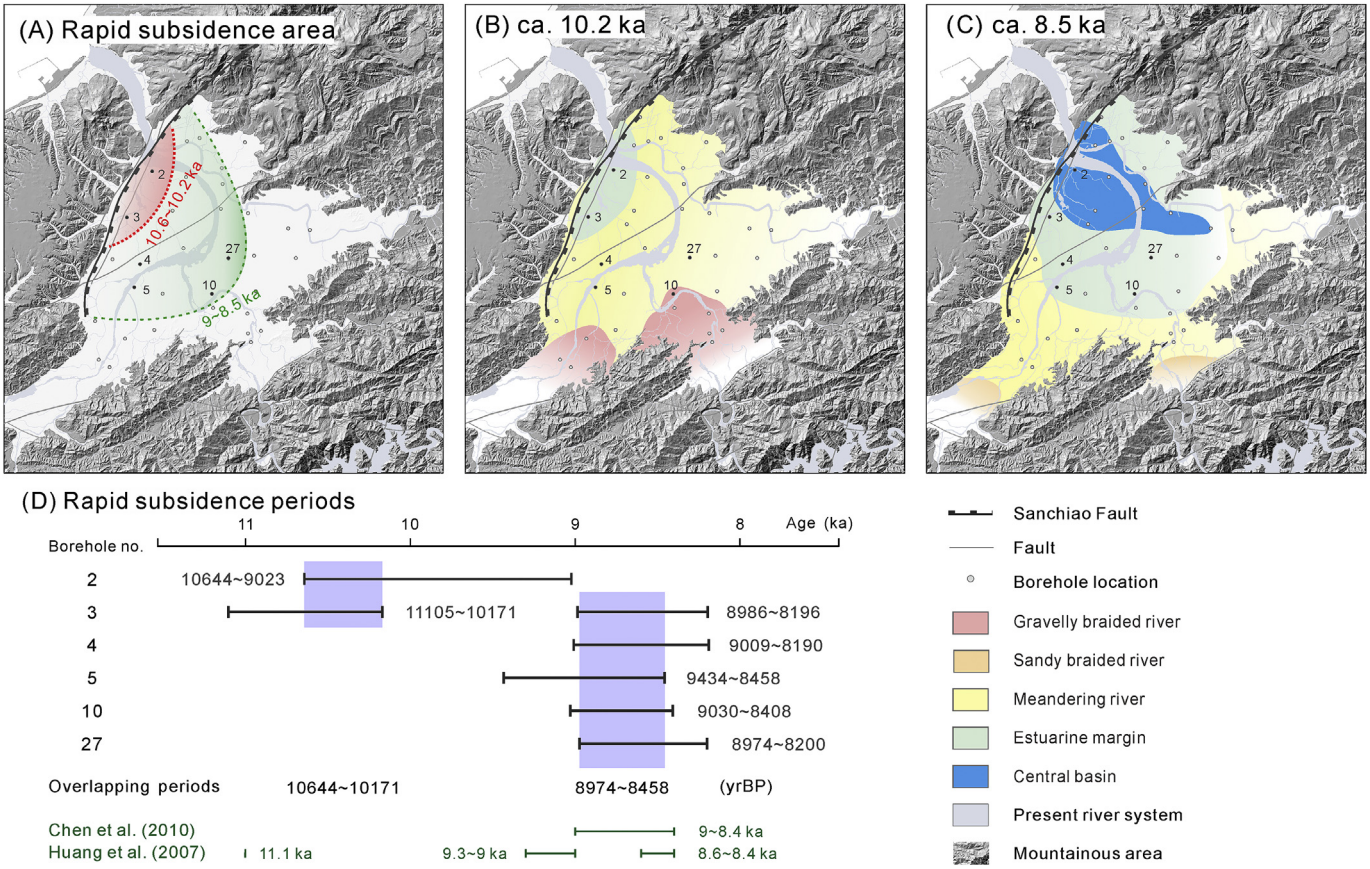


**Fig. 13.** Analysis of episodes of rapid basin subsidence 10.6–10.2 ka and 9–8.5 ka. (A) Areas of subsidence during the two rapid-subsidence phases, (B) spatial distribution of palaeoenvironments at 10.2 ka, (C) spatial distribution of palaeoenvironments at 8.5 ka and (D) time spans for rapid basin subsidence between 12 ka and 8 ka obtained from borehole nos. 2, 3, 4, 5, 10 and 27. For comparison, (D) also shows stages of rapid basin subsidence from Huang et al. (2007) and Chen et al. (2010a) The two time spans shaded in purple are interpreted as the two rapid-subsidence phases, which occurred between 10.6 ka and 10.2 ka and between 9 ka and 8.5 ka. (For interpretation of the references to colour in this figure legend, the reader is referred to the Web version of this article.)

## Acknowledgements

This work was supported by the Central Geological Survey [100-5226904000-02-05], the National Taiwan University and the Ministry of Science & Technology [MOST 105-2116-M-002-003; MOST 106-2116-M-002-004; MOST 106-2611-M-008-003]. Appreciation is due to Ping-Mei Liew of the National Taiwan University, Leh-Chyun Wu of the Chinese Culture University, Meng-Long Hsieh of the National Chung-Cheng University and Shu-fen Lin of the Academia Sinica for their inspiring discussions and suggestions.

## References

Abrahim, G.M.S., Nichol, S.L., Parker, R.J., Gregory, M.R., 2008. Facies depositional setting, mineral maturity and sequence stratigraphy of a Holocene drowned valley, Tamaki Estuary, New Zealand. Estuar. Coast. Shelf Sci. 79, 133–142.

Amato, V., Aucelli, P.P.C., Ciampo, G., Cinque, A., Di Donato, V., Pappone, G., Petrosino, P., Romano, P., Rosskopf, C.M., Russo Ermolli, E., 2013. Relative sea level changes and paleogeographical evolution of the southern Sele plain (Italy) during the Holocene. Quat. Int. 288, 112–128.

Amorosi, A., Colalongo, M.L., Pasini, G., Preti, D., 1999. Sedimentary response to Late Quaternary sea-level changes in the Romagna coastal plain (northern Italy). Sedimentology 46, 99–121.

Amorosi, A., Dinelli, E., Rossi, V., Vaiani, S.C., Sacchetto, M., 2008. Late quaternary palaeoenvironmental evolution of the adriatic coastal plain and the onset of Po river delta. Palaeogeogr. Palaeoclimatol. Palaeoecol. 268, 80–90.

Amorosi, A., Pacifico, A., Rossi, V., Ruberti, D., 2012. Late Quaternary incision and deposition in an active volcanic setting: the Volturno valley fill, southern Italy. Sediment. Geol. 282, 307–320.

Anthony, E.J., Lang, J., Oyede, L.M., 1996. Sedimentation in a tropical, microtidal, wave-dominated coastal-plain estuary. Sedimentology 43, 665–675.

Anthony, E.J., Oyede, L.M., Lang, J., 2002. Sedimentation in a fluvially infilling, barrier-bound estuary on a wave-dominated, microtidal coast: the Oueme River estuary, Benin, west Africa. Sedimentology 49, 1095–1112.

Bard, E., Hamelin, B., Delanghe-Sabatier, D., 2010. Deglacial meltwater pulse 1B and younger dryas sea levels revisited with boreholes at tahiti. Science 327, 1235–1237.

Bastos, A.C., Vilela, C.G., Quaresma, V.S., Almeida, F.K., 2010. Mid- to Late-Holocene estuarine infilling processes studied by radiocarbon dates, high resolution seismic and biofacies at Vitoria Bay, Espirito Santo, Southeastern Brazil. An. Da Acad. Bras. De. Ciencias 82, 761–770.

Bhandari, S., Maurya, D.M., Chamyal, L.S., 2005. Late Pleistocene alluvial plain sedimentation in lower narmada valley, western India: palaeoenvironmental implications. J. Asian Earth Sci. 24, 433–444.

Bird, M.I., Fifield, L.K., Teh, T.S., Chang, C.H., Shirlaw, N., Lambeck, K., 2007. An inflection in the rate of early mid-Holocene eustatic sea-level rise: a new sea-level curve from Singapore. Estuar. Coast. Shelf Sci. 71, 523–536.

Blum, M.D., Törnqvist, T.E., 2000. Fluvial responses to climate and sea-level change: a review and look forward. Sedimentology 47, 2–48.

Blum, M.D., Guccione, M.J., Wysocki, D.A., Robnett, P.C., Rutledge, E.M., 2000. Late Pleistocene evolution of the lower Mississippi River valley, southern Missouri to Arkansas. Geol. Soc. Am. Bull. 112, 221–235.

Bos, I.J., 2010. Architecture and facies distribution of organic-clastic lake fills in the fluvio-deltaic Rhine–Meuse system, The Netherlands. J. Sediment. Res. 80, 339–356.

Bosence, D.W.J., 1998. Stratigraphic and sedimentological models of rift basins. In: Purser, B., Bosence, D.J. (Eds.), Sedimentation and Tectonics in Rift Basins Red Sea:-Gulf of Aden. Springer Netherlands, pp. 9–25.

Boski, T., Moura, D., Veiga-Pires, C., Camacho, S., Duarte, D., Scott, D.B., Fernandes, S.G., 2002. Postglacial sea-level rise and sedimentary response in the Guadiana Estuary, Portugal/Spain border. Sediment. Geol. 150, 103–122.

Bruno, L., Bohacs, K.M., Campo, B., Drexler, T.M., Rossi, V., Sammartino, I., Scarponi, D., Hong, W., Amorosi, A., 2017. Early Holocene transgressive palaeogeography in the Po coastal plain (northern Italy). Sedimentology 64, 1792–1816.

Chang, J.-C., Shih, T.-T., Tseng, C.-H., Chen, M.L., Kao, P.F., 1989. A study of tidal effect on the lower course of Tanshui River. Geogr. Stud. 13, 1–55 (in Chinese with English abstract).

Chen, C.-H., Lin, S.-B., 2000. Distribution and significance of volcanic materials in sediments of the Taipei Basin. J. Geol. Soc. China 43, 287–310.

Chen, C.-T., Lee, J.-C., Chan, Y.-C., Lu, C.-Y., 2010a. Growth normal faulting at the western edge of the metropolitan Taipei Basin since the last glacial maximum, northern taiwan. Terr. Atmos. Ocean. Sci. 21, 409–428.

Chen, C.-T., Lee, J.-C., Chan, Y.-C., Lu, C.-Y., Teng, L.S.-Y., 2014. Elucidating the geometry of the active Shanchiao Fault in the Taipei metropolis, northern Taiwan, and the reactivation relationship with preexisting orogen structures. Tectonics 33, 2400–2418.

Chen, H.-W., Lee, T.-Y., Wu, L.-C., 2010b. High-resolution sequence stratigraphic analysis of Late Quaternary deposits of the Changhua Coastal Plain in the frontal arc-continent collision belt of Central Taiwan. J. Asian Earth Sci. 39, 192–213.

Chen, W.-S., Lin, C.-C., Yang, C.-C., Fei, L.-Y., Shieh, K.-S., Kung, H.-M., Lin, P.-Y., Yang, S.-C., 2008. The temporal and spatial evolution of sedimentary sequence framework and tectonics of the Taipei Basin since the Late-Pleistocene. Bull. Central Geol. Surv. 21, 61–106 (in Chinese, with English abstract).

Chen, Y.-G., Liu, T.-K., 1996. Sea level changes in the last several thousand years, Penghu Islands, Taiwan Strait. Quat. Res. 45, 254–262.

Dabrio, C.J., Zazo, C., Goy, J.L., Sierro, F.J., Borja, F., Lario, J., González, J.A., Flores, J.A., 2000. Depositional history of estuarine infill during the last postglacial transgression Gulf of Cadiz, Southern Spain. Mar. Geol. 162, 381–404.

Dadson, S.J., Hovius, N., Chen, H., Dade, W.B., Hsieh, M.-L., Willett, S.D., Hu, J.-C., Horng, M.-J., Chen, M.-C., Stark, C.P., Lague, D., Lin, J.-C., 2003. Links between erosion, runoff variability and seismicity in the Taiwan orogen. Nature 426, 648–651.

Dalrymple, R.W., Zaitlin, B.A., Boyd, R., 1992. Estuarine facies models: conceptual basis and stratigraphic implications. J. Sediment. Res. 62, 1130–1146.

Doglioni, C., Dagostino, N., Mariotti, G., 1998. Normal faulting vs regional subsidence and sedimentation rate. Mar. Petroleum Geol. 15, 737–750.

Fagel, N., Alleman, L.Y., Granina, L., Hatert, F., Thamo-Bozso, E., Cloots, R., André, L., 2005. Vivianite formation and distribution in Lake Baikal sediments. Glob. Planet. Change 46, 315–336.

Fairbanks, R.G., 1989. A 17000 year glacio-eustatic sea level record: influence of glacial melting rates on the Younger Dryas event and deep-ocean circulation. Nature 342, 637–642.

Fornari, M., Giannini, P.C.F., Nascimento, D.R., 2012. Facies associations and controls on the evolution from a coastal bay to a lagoon system, Santa Catarina Coast, Brazil. Mar. Geol. 323–325, 56–68.

Fuller, I.C., Macklin, M.G., Lewin, J., Passmore, D.G., Wintle, A.G., 1998. River response to high-frequency climate oscillations in southern Europe over the past 200 k.y. Geology 26, 275–278.

Gobo, K., Ghinassi, M., Nemec, W., Sjursen, E., Hampson, G., 2014. Development of an incised valley-fill at an evolving rift margin: Pleistocene eustasy and tectonics on the southern side of the Gulf of Corinth, Greece. Sedimentology 61, 1086–1119.

Goodbred Jr., S.L., Kuehl, S.A., 2000. The significance of large sediment supply, active tectonism, and eustasy on margin sequence development: late Quaternary stratigraphy and evolution of the Ganges–Brahmaputra delta. Sediment. Geol. 133, 227–248.

Granja, H., Rocha, F., Matias, M., Moura, R., Caldas, F., Marques, J., Tareco, H., 2010. Lagoa da Apúlia: a residual lagoon from the Late Holocene (NW coastal zone of Portugal). Quat. Int. 221, 46–57.

Hanebuth, T., Stattegger, K., Grootes, P.M., 2000. Rapid flooding of the Sunda Shelf: a late-glacial sea-level record. Science 288, 1033–1035.

Heap, A.D., Nichol, S.L., 1997. The influence of limited accommodation space on the stratigraphy of an incised-valley succession: weiti River estuary, New Zealand. Mar. Geol. 144, 229–252.

Hijma, M.P., Cohen, K.M., Hoffmann, G., van der Spek, A.J.F., Stouthamer, E., 2009. From river valley to estuary: the evolution of the Rhine mouth in the early to middle Holocene (western Netherlands, Rhine-Meuse delta). Neth. J. Geosciences 88, 13–53.

Holz, M., 2003. Sequence stratigraphy of a lagoonal estuarine system—an example from the lower permian rio bonito formation, paraná basin, Brazil. Sediment. Geol. 162, 305–331.

Hong, E., Poan, H.-L., Liu, H.-C., Lai, T.-H., Huang, C.-C., Fei, L.-Y., 2006. The sedimentary facies and paleoenvironment analysis of the Taipei basin. West. Pac. Earth Sci. 6, 59–86 (in Chinese, with English abstract).

Hori, K., Saito, Y., Zhao, Q., Cheng, X., Wang, P., Sato, Y., Li, C., 2001. Sedimentary facies of the tide-dominated paleo-Changjiang (Yangtze) estuary during the last transgression. Mar. Geol. 177, 331–351.

Hsieh, M.-L., Lai, T.-H., Wu, L.-C., Lu, W.-C., Liu, H.-T., Liew, P.-M., 2006. Eustatic sea-level change of 11-5 ka in western Taiwan, constrained by radiocarbon dates of core sediments. Terr. Atmos. Ocean. Sci. 17, 353–370.

Hsieh, M.L., Lee, C.-Y., Wang, C.-M., Chen, B.-C., Su, P.-J., 2016. The Culmination of Holocene Sea Level in the Taipei Basin: Evidence from Fossil Mangrove forest by the Hsin-dian River Upstream of the Fu-ho Bridge. Taiwan Geosciences Assembly, Taipei ST2–3A-05 (in Chinese).

Hsu, M.-H., Wu, C.-R., Liu, W.-C., Kuo, A.Y., 2006. Investigation of turbidity maximum in a mesotidal estuary, Taiwan. J. Am. Water Resour. Assoc. 42, 901–914.

Huang, C.-Y., 2006. On foraminifers of Taipei Basin. West. Pac. Earth Sci. 6, 29–58 (in Chinese, with English abstract).

Huang, S.-Y., Rubin, C.M., Chen, Y.-G., Liu, H.-C., 2007. Prehistoric earthquakes along the shanchiao fault, Taipei Basin, northern taiwan. J. Asian Earth Sci. 31, 265–276.

Huang, T.-C., 1962. The sungshan formation in the Taipei Basin. Mem. Geol. Soc. China 1, 133–151.

Kitazawa, T., 2007. Pleistocene macrotidal tide-dominated estuary–delta succession, along the Dong Nai River, southern Vietnam. Sediment. Geol. 194, 115–140.

Leorri, E., Fatela, F., Drago, T., Bradley, S.L., Moreno, J., Cearreta, A., 2013. Lateglacial and Holocene coastal evolution in the Minho estuary (N Portugal): Implications for understanding sea-level changes in Atlantic Iberia. The Holocene 23, 353–363.

Lin, C.-W., Lu, S.-T., Shih, T.-S., Chen, Z.-Y., Lin, Y.-H., 2007. Sanchiao Fault. In: Special Publication of the Central Geological Survey, vol 19. pp. 7–32 (in Chinese).

Liu, J.P., Milliman, J.D., 2004. Reconsidering Melt-water Pulses lA and lB: global impacts of rapid sea-level rise. J. Ocean Univ. China 3, 183–190.

Liu, T.-K., 1995. The Study of Radiocarbon Dates and Groundwater Quality, the Comprehensive Survey on the Subsurface Geology and Engineering Environment in Taipei Basin. Central Geological Survey, Taipei, pp. 38 (in Chinese).

Liu, T.K., Chen, Y.G., Wu, W.S., Lo, C.T., Wei, K., 1994. An implication of the ages of sediments and groundwater from Taipei Basin, Taiwan. In: Joint Symposium of Taiwan Quaternary 5th & Investigation of Subsurface Geology and Engineering Environments of Taipei Basin, Taipei, pp. 143–146 (in Chinese, with English abstract).

Maddy, D., Bridgland, D., Westaway, R., 2001. Uplift-driven valley incision and climate-controlled river terrace development in the Thames Valley, UK. Quat. Int. 79, 23–36.

Miall, A.D., Arush, M., 2001. Cryptic sequence boundaries in braided fluvial successions. Sedimentology 48, 971–985.

Milli, S., D'Ambrogi, C., Bellotti, P., Calderoni, G., Carboni, M.G., Celant, A., Di Bella, L., Di Rita, F., Frezza, V., Magri, D., Pichezzi, R.M., Ricci, V., 2013. The transition from wave-dominated estuary to wave-dominated delta: the Late Quaternary stratigraphic architecture of Tiber River deltaic succession (Italy). Sediment. Geol. 284–285, 159–180.

Muto, T., Steel, R.J., 1997. Principles of regression and transgression; the nature of the interplay between accommodation and sediment supply. J. Sediment. Res. 67, 994–1000.

Muto, T., Steel, R.J., 2002. In defense of shelf-edge delta development during falling and lowstand of relative sea level. J. Geol. 110, 421–436.

Nichol, S.L., Zaitlin, B.A., Thom, B.G., 1997. The upper hawkesbury river, new south wales, Australia: a Holocene example of an estuarine bayhead delta. Sedimentology 44, 263–286.

Nichols, G.J., Fisher, J.A., 2007. Processes, facies and architecture of fluvial distributary system deposits. Sediment. Geol. 195, 75–90.

Nriagu, J.O., 1972. Stability of vivianite and ion-pair formation in the system Fe3(PO4)2-H3PO4H3PO4-H2O. Geochimica Cosmochimica Acta 36, 459–470.

Peng, C.-H., Teng, L.S., Yuan, P.B., 1999. Facies characteristics of Taipei Basin deposits. Special Publ. Central Geol. Surv. 1999, 67–99 (in Chinese, with English abstract).

Reimer, P.J., Bard, E., Bayliss, A., Beck, J.W., Blackwell, P.G., Bronk Ramsey, C., Buck, C.E., Cheng, H., Edwards, R.L., Friedrich, M., Grootes, P.M., Guilderson, T.P., Haflidason, H., Hajdas, I., Hatté, C., Heaton, T.J., Hoffmann, D.L., Hogg, A.G., Hughen, K.A., Kaiser, K.F., Kromer, B., Manning, S.W., Niu, M., Reimer, R.W., Richards, D.A., Scott, E.M., Southon, J.R., Staff, R.A., Turney, C.S.M., van der Plicht, J., 2013. IntCal13 and Marine13 radiocarbon age calibration curves 0-50,000 years cal BP. Radiocarbon 55, 1869–1887.

Ricci Lucchi, M., Fiorini, F., Luisa Colalongo, M., Vittorio Curzi, P., 2006. Late-Quaternary paleoenvironmental evolution of Lesina lagoon (southern Italy) from subsurface data. Sediment. Geol. 183, 1–13.

Roberts, H.H., 1998. Delta switching: early responses to the Atchafalaya River diversion. J. Coast. Res. 14, 882–899.

Rosenquist, I.T., 1970. Formation of vivianite in Holocene clay sediments. Lithos 3, 327–334.

Rossetti, D.F., Santos Júnior, A.E., 2004. Facies architecture in a tectonically influenced estuarine incised valley fill of Miocene age, northern Brazil. J. S. Am. Earth Sci. 17, 267–284.

Roy, P.S., 1984. New south wales estuaries - Their origin and evolution. In: Thom, B.G. (Ed.), Developments in Coastal Geomorphology in Australia. Academic Press, Sydney, pp. 99–121.

Roy, P.S., Thom, B.G., Wright, L.D., 1980. Holocene sequences on an embayed high-energy coast: an evolutionary model. Sediment. Geol. 26, 1–19.

Schlische, R.W., 1991. Half-graben basin filling models: new constraints on continental extensional basin development. Basin Res. 3, 123–141.

Shieh, Y.-T., 2001. A preliminary study of the foraminifer assemblages in the KT-1 observation well in the Taipei Basin and their paleoenvironmental implications. Bull. Central Geol. Surv. 14, 83–102 (in Chinese, with English abstract).

Shieh, Y.-T., 2006. Paleoenvironmental implications of the Quaternary sequence and its foraminiferal assemblages in the east part of Taipei basin. West. Pac. Earth Sci. 6, 115–127 (in Chinese, with English abstract).

Shih, R.-C., Lin, C.-W., Liu, H.-C., Lu, S.-T., 2006. Northward extension of the Sanchiao fault in northern Taiwan from the shallow seismic reflection images. West. Pac. Earth Sci. 6, 149–168.

Sloss, C.R., Jones, B.G., Switzer, A.D., Nichol, S., Clement, A.J.H., Nicholas, A.W., 2010. The Holocene infill of Lake Conjola, a narrow incised valley system on the southeast coast of Australia. Quat. Int. 221, 23–35.

Song, S.-R., Chen, T.-M., Tsao, S., Chen, H.-F., Liu, H.-C., 2007. Lahars in and around the Taipei basin: implications for the activity of the Shanchiao fault. J. Asian Earth Sci. 31, 277–286.

Stuiver, M., Braziunas, T.F., 1993. Modeling atmospheric 14C influences and 14C ages of marine samples to 10,000 BC. Radiocarbon 35, 137–189.

Stuiver, M., Reimer, P.J., Reimer, R.W., 2016. CALIB Radiocarbon Calibration, 7.0.4 Ed. (Northern Ireland, UK).

Su, P.-J., Lin, A.T., Hu, J.-C., 2016. New definition of lithofacies and sedimentary environment of the Jingmei formation, Taipei Basin. Bull. Central Geol. Surv. 29, 173–196 (in Chinese, with English abstract).

Su, P.-J., Chi, T.-C., Fei, L.-Y., Su, T.-W., Teng, L.S., 2018. Facies characteristics and depositional history of the sungshan formation, Taipei Basin. in press. West. Pac. Earth Sci (in Chinese, with English abstract).

Ta, T.K.O., Nguyen, V.L., Tateishi, M., Kobayashi, I., Saito, Y., Nakamura, T., 2002. Sediment facies and Late Holocene progradation of the Mekong River Delta in Bentre Province, southern Vietnam: an example of evolution from a tide-dominated to a tide- and wave-dominated delta. Sediment. Geol. 152, 313–325.

Tanabe, S., Nakanishi, T., Matsushima, H., Hong, W., 2013. Sediment accumulation patterns in a tectonically subsiding incised valley: insight from the Echigo Plain, central Japan. Mar. Geol. 336, 33–43.

Tanabe, S., Nakanishi, T., Ishihara, Y., Nakashima, R., 2015. Millennial-scale stratigraphy of a tide-dominated incised valley during the last 14 kyr: spatial and quantitative reconstruction in the Tokyo Lowland, central Japan. Sedimentology 62, 1837–1872.

Teng, L.S., Lee, C.-T., Peng, C.-H., Chen, W.-F., Chu, C.-J., 2001. Origin and geological evolution of the Taipei Basin, northern taiwan. West. Pac. Earth Sci. 1, 115–142.

Teng, L.S., Liu, T.-K., Chen, Y.-G., Liew, P.-M., Lee, C.-T., Liu, H.-C., Peng, C.-H., 2004. Influence of tahan river capture over the Taipei Basin. Geogr. Res. 41, 61–78 (in Chinese, with English abstract).

Teng, L.S., Song, S.-R., Liou, T.-S., Hsiao, T.-H., Lee, C.T., Jhuang, J.-M., 2008. Volcaniclastic deposits of the northern Linkou Tableland. West. Pac. Earth Sci. 8, 43–75 (in Chinese, with English abstract).

Teng, L.S., Wang, S.-C., Chang, J.-B., Hsu, C., Yuan, P.B., Chen, P.-Y., 1994. Stratigraphic architectures of the Quaternary Taipei Basin. In: The Joint Symposium on Taiwan Quaternary [5] and on Investigation of Subsurface geology/engineering Environment of Taipei Basin. Central Geological Survey, Chungho 192–135 (in Chinese).

Teng, L.S., Yuan, P.B., Yu, N.-T., Peng, C.-H., 2000. Sequence stratigraphy of the Taipei Basin deposits: a preliminary study. J. Geol. Soc. China 43, 497–520.

Tesson, M., Labaune, C., Gensous, B., Suc, J.P., Melinte-Dobrinescu, M., Parize, O., Imbert, P., Delhaye-Prat, V., 2011. Quaternary "compound" incised valley in a microtidal environment, Roussillon continental shelf, western Gulf of Lions, France. J. Sediment. Res. 81, 708–729.

Törnqvist, T.E., 1993. Holocene alternation of meandering and anastomosing fluvial systems in the Rhine-Meuse Delta (central Netherlands) controlled by sea-level rise and subsoil erodibility. J. Sediment. Res. 63, 683–693.

Traini, C., Menier, D., Proust, J.N., Sorrel, P., 2013. Transgressive systems tract of a ria-type estuary: the Late Holocene Vilaine River drowned valley (France). Mar. Geol. 337, 140–155.

Tsao, S.-J., Song, S.-R., Lee, C.-Y., 2001. Geological implications of lahar deposits in the Taipei Basin. West. Pac. Earth Sci. 1, 199–212.

Tsao, S., Song, S.-R., Lee, C.-Y., Wang, Y.S., Hsu, M.-I., Lin, M.-C., Su, T.-W., 1999. Preliminary study of the lahar deposits of the kuandu Well-1 in the Taipei Basin. Bull. Central Geol. Surv. 13, 103–118 (in Chinese, with English abstract).

Tseng, M.-H., Liew, P.-M., 1999. A preliminary probe on sporo-pollen assemblages and paleoenvironments of the recent 20ka in Taipei Basin. Special Publ. Central Geol. Surv. 11, 159–179 (in Chinese, with English abstract).

Waelbroeck, C., Labeyrie, L., Michel, E., Duplessy, J.C., McManus, J.F., Lambeck, K., Balbon, E., Labracherie, M., 2002. Sea-level and deep water temperature changes derived from benthic foraminifera isotopic records. Quat. Sci. Rev. 21, 295–305.

Wang-Lee, C.-M., Cheng, Y.-M., Wang, Y., 1987. Geology of the Taipei Basin. Taiwan Min. Industry 30, 350–380 (in Chinese).

Wei, K., Chen, Y.-G., Liu, T.-K., 1998. Sedimentary history of the Taipei Basin with constraints from thermoluminescence dates. J. Geol. Soc. China 41 190–125.

Wentworth, C.K., 1922. A scale of grade and class terms for clastic sediments. J. Geol. 30, 377–392.

Willis, A., 2000. Tectonic control of nested sequence architecture in the sego sandstone, neslen formation and upper castlegate sandstone (upper cretaceous), sevier foreland basin, Utah, USA. Sediment. Geol. 136, 277–317.

Wilson, K., Berryman, K., Cochran, U., Little, T., 2007. A Holocene incised valley infill sequence developed on a tectonically active coast: pakarae River, New Zealand. Sediment. Geol. 197, 333–354.